Top Organomet Chem (2014) 48: 319–370
DOI: 10.1007/3418_2014_83

Published online: 4 May 2014

Organometallic Ruthenium Nanoparticles and Catalysis

Karine Philippot, Pascal Lignier, and Bruno Chaudret

Abstract Due to a high number of possible applications in various domains, metal nanoparticles are nowadays the subject of an extensive development. This interest in metal nanoparticles is related to their electronic properties at the frontier between those of molecular species and bulk compounds which are induced by their nanometric size. Regarding the field of catalysis, the growing attention for metal nanoparticles also results from the high proportion of surface atoms present in the upper layer of the metallic core which gives rise to numerous potential active sites. Thus, nanocatalysis (which involves the use of catalysts with at least one dimension at the nanoscale) has emerged in the field of modern catalysis as a domain on the borderline between homogeneous and heterogeneous catalysis. Present developments aim at multifunctionality which can be achieved by the proper design of complex nanostructures also named nanohybrids. In nanohybrid the term "hybrid" refers to the appropriate association between a metal core and a stabilizing shell such as a polymer, a ligand, an ionic liquid, or even a support (inorganic materials, carbon black, carbon nanotubes, etc.. . .). This association can be considered as crucial to tune the surface properties of nanostructures and consequently their catalytic performance. The main expectation for the scientific community is that precisely designed nanoparticles (in terms of size, shape, and composition including surface ligands) should offer the benefits of both homogeneous and heterogeneous catalysts, namely high efficiency and better selectivity.

K. Philippot (✉) and P. Lignier
Laboratoire de Chimie de Coordination, CNRS, LCC, 205 Route de Narbonne, 31077 Toulouse, France

Université de Toulouse, UPS, INPT, LCC, 31077 Toulouse, France
e-mail: karine.philippot@lcc-toulouse.fr

B. Chaudret
Laboratoire de Physique et Chimie des Nano-Objets (LPCNO), UMR5215 INSA-CNRS-UPS, Institut des Sciences appliquées, 135, Avenue de Rangueil, 31077 Toulouse, France

In that context, we have been developing an efficient and versatile synthesis method using common tools from organometallic chemistry to produce well-controlled nanostructures which have been proved to be of interest for application in catalysis. A high number of studies have been focused on ruthenium nanosystems due to the use of a very convenient organometallic precursor, namely [Ru(COD)(COT)], as the metal source. This Ru complex is easily decomposed under dihydrogen atmosphere at room temperature. In addition, it is a complex of choice to prepare "naked" ruthenium nanostructures since the olefinic ligands present in the coordination sphere of ruthenium are hydrogenated into alkanes which exhibit no interaction with the metal surface. As a consequence, the metallic surface of the obtained nanoparticles is only covered by hydrides and the stabilizer which was deliberately added. This is highly convenient for studying the influence of the stabilizer on the morphology of the nanoparticles as well as their surface chemistry and related catalytic performance.

This chapter gives an overview of our experience in the preparation of ruthenium nanoparticles of controlled size and surface state. Insights are given on the study of their surface chemistry by using simple techniques, mainly IR and NMR, both in solution and in solid state, as well as model hydrogenation reactions. We also discuss the performances of the Ru nanoparticles in catalysis which have been investigated both in solution (in organic or aqueous phases) and after their deposition on a support (alumina, silica, or carbon supports).

Keywords Catalysis · Colloid · Ligand · Nanocluster · Nanohybrid · Nanoparticle · Nanostructure · Organometallic synthesis · Ruthenium · Surface chemistry

Contents

1 Introduction

Due to a high number of potential applications in various fields such as opto-electronics, sensors, medicine, catalysis [1, 2], metal nanoparticles, also named nanoclusters, nanostructures or colloids are nowadays the subject of an extensive development. This growing attention for metal nanoparticles (MNPs) results mainly from their particular electronic properties induced by their nanometric size and situated at the frontier between those of molecular species and bulk compounds. Present developments aim at multifunctionality at the nanoscale and this can be achieved by the proper design of nanohybrids. In nanohybrids, the term "hybrid" refers to the appropriate association between a metal core and a stabilizing shell which can be a polymer, a ligand, or even a support. This association can be considered as a key parameter to tune the surface properties of nanostructures. When catalysis is the target application, the high proportion of surface atoms present in the upper layer of metal nanoparticles is also of high interest since it gives rise to numerous potential active sites [3–6]. Thus, in the modern area of catalysis, nanocatalysis which involves the use of catalysts with at least one dimension at the nanoscale has emerged as a domain on the borderline between homogeneous and heterogeneous catalysis [7–11]. The main expectation for the scientific community is that precisely designed nanoparticles (in terms of size, shape, and composition including surface ligands) should offer the benefits of both homogeneous and heterogeneous catalysts, namely high efficiency and better selectivity.

For applications in catalysis, the production of metal nanoparticles mainly deals with (1) chemical or electrochemical reduction of the corresponding metal salts, (2) decomposition of organometallic complexes through reduction and/or displacement of ligands from the coordination sphere. These syntheses require the presence of a stabilizer (also called capping agent) [12, 13] which can be a wide range of functional organic ligands [14, 15], surfactants [16], polymers [17, 18], dendrimers [19–21], ionic liquids [22, 23], inorganic ligands [24] as reported in the literature. The choice of the stabilizing agent is crucial since this can influence the nucleation, growth, stability, and surface chemistry of MNPs [25]. Thus, the synthesis and characterization of metal-based nanocatalysts have experienced a huge development during the past decade, e.g., to determine the influence of the stabilizer on the catalytic properties. Since the surface properties of MNPs are related to their size, shape, crystalline structure, chemical composition, efficient synthetic methods are required to have MNPs of well-defined characteristics. This will enable to precisely

study the influence of MNP morphology on their surface properties and catalytic performances. In parallel to these methods for the preparation of MNPs, heterogeneous catalysis has developed powerful tools to model and characterize the surface of the nanoparticles. Interestingly, these studies can be achieved during the catalytic process (Transmission Electron Microscopy (TEM), powder X-Ray Diffraction (DRX), X-ray Photoelectron Spectrometry (XPS), Extended X-Ray Absorption Fine Structure (EXAFS), IR in operando) [26–34]. However, simple spectroscopic methods, such as UV/Vis, IR, or NMR both in solution and in solid state, which are adapted from molecular chemistry and homogeneous catalysis, offer interesting alternatives to precisely characterize the metallic surface of MNPs.

For 25 years, our team has been developing a versatile approach for the synthesis of metal nanoparticles starting from organometallic precursors. This approach was inspired by previous results on the preparation of hydrogen-rich complexes [35]. It takes advantage of previous knowledge on organometallic complexes which are not very thermally stable, and prone to oxidation, sometimes energetically. This leads to the formation of black solutions or residues as observed for various metals. Whilst these observations seemed very detrimental for molecular reactions, this has prompted chemists to take profit of this decomposition tendency. As a consequence, organometallic complexes have been used as precursors for the preparation of metal nanoparticles. Since organometallic derivatives are not always easy to prepare and most often sensitive to both air and moisture, this may seem both senseless and expensive to decompose them to prepare metal nanoparticles. However, this approach exhibits two main advantages. First, their decomposition requires milder conditions which allow a better control of the nanoparticle formation. Second, organometallic derivatives offer access to clean procedures which avoid the presence of contaminants such as salts, halides, main group oxides, on the surface of the nanostructures [36, 37].

The interest of high energy organometallic complexes to synthesize otherwise inaccessible species was demonstrated in the early 1980s by John Spencer who reported the synthesis of polyhydrido platinum clusters from platinum (0) olefin complexes [38, 39]. This work served as an inspiration for the subsequent synthesis of polyhydrido ruthenium complexes. Besides the bis(styrene) ruthenium derivative, $[Ru(C_8H_8)_2(PPh_3)_{2]}$ [40], the scope of which was found to be too limited, the possibility of using a new ruthenium(0) complex [Ru(COD)(COT)] (COD = 1,5-cyclooctadiene; COT = 1,3,5-cyclooctatriene) was explored [41]. This resulted in the preparation of the $[RuH_2(H_2)_2(PCy_3)_2]$ complex at room temperature by bubbling dihydrogen into a solution containing the [Ru(COD)(COT)] precursor and two molar equivalents of a bulky phosphine, PCy_3 [35]. When testing the generality of this synthesis, it was noticed that in certain cases the solution turned black and that, in the absence of any ligand, a black deposit of pyrophoric ruthenium powder precipitated. Following this observation, and fascinated by previous pioneering works (see, for example, the works of Chini et al. on very large organometallic clusters [42–44], Basset et al. on the use of organometallic complexes to prepare heterogeneous catalysts [45], Schmid et al. on the preparation of Gold 55 clusters through borane reduction of

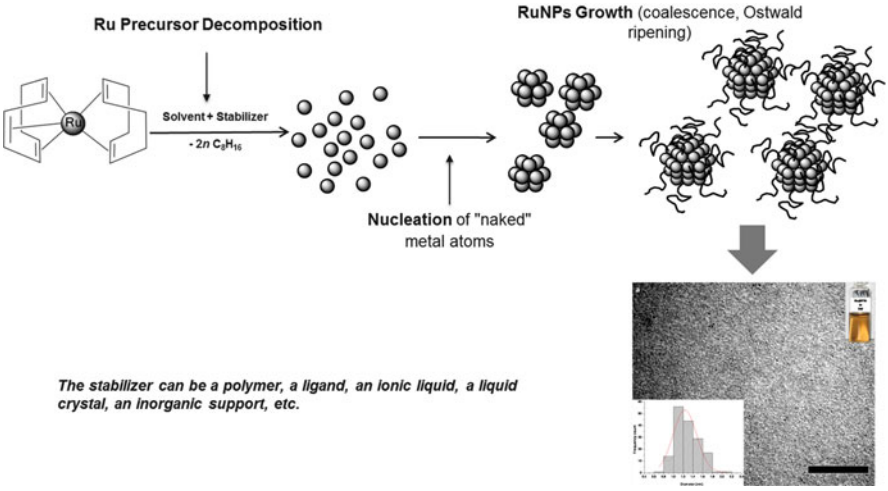

Fig. 1 Synthesis of ruthenium nanoparticles from [Ru(COD)(COT)] organometallic precursor. (Adapted from [37] with permission from the CNRS and RSC)

$AuCl(PPh_3)$ (see for example: [46–50]), and Bradley et al. who decomposed carbonyl clusters to produce nanoparticles in solution [51]), we attempted the controlled decomposition of [Ru(COD)(COT)] in the presence of various stabilizers in order to prepare hydride containing large clusters. As a result, we first obtained diverse polymer-stabilized ruthenium nanoparticles (RuNPs) and then extended the approach to both different stabilizers (mainly ligands) and different metals [52]. Thus, in addition to noble metals (Au, Ag, Pt, Rh, Pd, Ru) which are of interest in catalysis, this approach could be extended to magnetic metals (Fe, Co, Ni, and their alloys) via a judicious choice of precursors. The resulting materials may display interesting magnetic properties for potential applications as hard magnets which are relevant for tunnel magnetoresistance or for hyperthermia. In addition copper may be used for applications in micro-electronics (see for example: [53–57]). This implies to employ precursors, such as [Co(COE)(COD)], $[Ni(COD)_2]$; COE = cyclooctenyle, which are similar to [Ru(COD)(COT)]. Aryl $(Cu(Mes)_4$; Mes = mesityle) and amido $(M[N(SiMe_3)_2]_2$; M = Fe, Co) complexes are also relevant. For example, the amine ligand could be easily displaced from the nanoparticle surface.

About ruthenium, a strong activity has been maintained all over the years since ruthenium is a metal of interest in catalysis (it is a very good hydrogenation and oxidation catalyst). In addition, ruthenium can easily accommodate ligands which allow us to study the influence of ligands on the growth of nanoparticles. Furthermore, this metal hardly displays any Knight shift which makes it a metal of choice to study the coordination of the ligand by solution or solid-state NMR. Finally, the olefinic complex [Ru(COD)(COT)] is particularly convenient since its decomposition easily occurs below room temperature (RT) under low dihydrogen pressure (Fig. 1). Under dihydrogen, the unsaturated ligands present in the coordination

sphere are reduced in corresponding alkanes which are inert towards the metallic surface and thus do not interact with the growing nanoparticles. As a consequence, Ru(COD)(COT)] is a source of "naked" Ru atoms in very mild conditions in solution. The resulting particles are, however, not totally naked since they are covered with hydrides (resulting from the synthesis conditions). In addition, the nanoparticles interact with the added stabilizers present in solution. This makes possible to precisely tune the surface properties of metal nanoparticles by an appropriate choice of the stabilizer as discussed later. Then, the question is related to the stabilization of the nanoparticles. What do we need to stabilize nanoparticles, allow them to react but not to coalesce up to the point where they will agglomerate and precipitate? The ruthenium is again ideal since there are only hydrides on the ruthenium surface. This enables us to study a wide range of stabilizers including the stabilizing agents which exhibit very weak interactions with the metal surface.

In this chapter, we present an overview of our experience in the organometallic synthesis of ruthenium nanoparticles of controlled size and surface state. We also give insights on the study of their surface chemistry by using simple techniques, mainly IR and NMR both in solution and in solid state. In addition, model hydrogenation reactions have been used. We also discuss the performances of these materials as catalysts in solution (organic and aqueous phases) and on a support (alumina, silica, or carbon materials).

2 Organometallic Synthesis of RuNPs and Surface Chemistry Studies

2.1 Polymer-Stabilized RuNPs

Polymers have long been used to stabilize metal nanoparticles giving rise to a steric protection [58]. In fact, an organic polymer may display a structure containing voids which results in the formation of "nanoreactors" inside which the nanoparticles can grow depending on the amount of precursor present. As a consequence, the size distribution of the particles is controlled by the concentration of the solution as well as both the size and monodispersity of these "nanoreactors." In these cases, the nanoparticles display little or no chemical interaction with the polymer, i.e. they are ligand-free except both solvent and hydrogen. These materials appear ideal for catalysis and surface studies.

Our synthesis procedure was developed originally using [Ru(COD)(COD)] as a precursor under mild conditions of pressure and temperature (3 bar H_2, RT). The dihydrogen atmosphere acts as a reducing agent in the presence of a polymer (Fig. 2), namely nitrocellulose (NC), cellulose acetate (CA), or polyvinylpyrrolidone (PVP). The hydrogen treatment allows the reduction of the olefin ligands of the ruthenium precursor into cyclooctane which is inert towards the metal surface. This is a crucial point since the metal surface of these polymer-stabilized

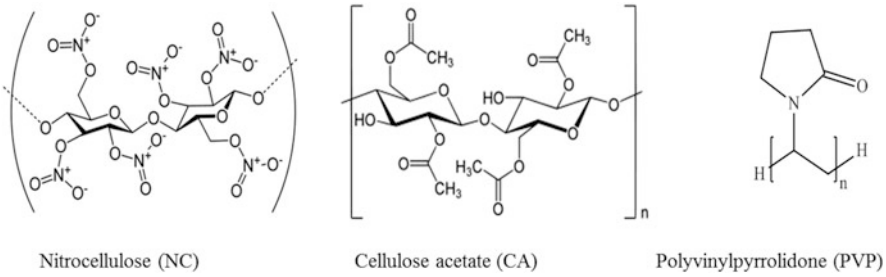

Fig. 2 Formula of polymers used for the synthesis of polymer-stabilized RuNPs

systems is "naked". In collaboration with J. Bradley, we showed that nanoparticles of ruthenium of very small size (ca. 1 nm) could be obtained by bubbling hydrogen through a solution of [Ru(COD)(COT)] in THF in the presence of PVP. Interestingly, intriguing ^{13}C NMR results were obtained following the addition of ^{13}CO [59]. The preparations of RuNPs stabilized by nitrocellulose and cellulose acetate were the first results entirely obtained in the group on this topic [60]. The resulting nanoparticles were very small in size, exhibiting a mean diameter between 1 and 2 nm, which depends on both the nature of the polymeric matrix and the metal/polymer ratio (wt.%). These results showed that small RuNPs can remain well dispersed in the reaction medium using polymers which weakly interact with this surface.

The stable nanoparticles were used to study the surface reactivity of nano-objects. To probe the surface state of these RuNPs, the adsorption of carbon monoxide (CO) was studied by IR. This shows that CO can coordinate at the surface of the particles in two different coordination modes: linear at 2,030 cm^{-1} and bridging at 1,968 cm^{-1}.

The synthesis of RuNPs in the presence of polyvinylpyrrolidone was then revisited using our now standard procedure (3 bar H_2) giving rise to 1.1 nm nanoparticles (Fig. 3) [61].

Characterization by WAXS showed crystalline nanoparticles displaying the expected hexagonal close packed (hcp) structure of bulk ruthenium. Reactivity studies were carried out in particular with CO to show the availability of the nanoparticles surface for reactivity. Recently, the synthesis of these PVP-stabilized RuNPs has been reproduced to perform an exhaustive study of the coordination of CO to their surface by a combination of IR and NMR techniques [62]. It has been observed that: (1) the coordination mode of the CO to the NP surface depends on the reaction time and (2) CO is mobile. Low reaction-times give rise to CO adsorption in the bridging mode while longer reaction times result in the adsorption of more CO molecules only adsorbed in the linear or multicarbonyle modes.

These PVP-stabilized RuNPs were also shown to be of interest for chemical transformations. In a recent work with Rousseau et al., these NPs appeared as a highly active catalyst for the deuteration of nitrogen-containing compounds [63].

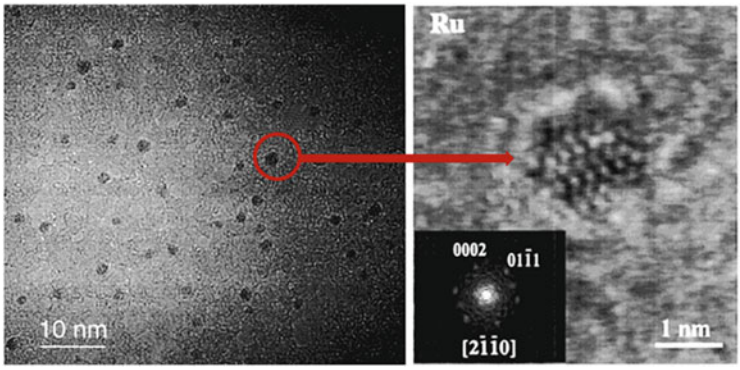

Fig. 3 TEM (*left*) and HRTEM (*right*) micrographs of RuNPs in PVP. (Reproduced from [61] with permission from ACS)

In the presence of D_2 as the isotopic source, the PVP-stabilized RuNPs allowed an efficient H/D exchange which resulted in the deuteration of a large diversity of aza compounds such as pyridines, quinolines, indoles, and alkyl amines. A total of 22 compounds could be isotopically labeled in good yields with high chemo- and regioselectivities following a simple procedure, i.e. mild reaction conditions (1–2 bar of D_2; 55°C) and simple filtration to recover the labeled product. The viability of this procedure was demonstrated by the labeling of eight biologically active compounds. Remarkably, conservation of the enantiomeric purity of the labeled compounds was observed, even though labeling took place in the vicinity of the asymmetric center. The level of isotopic enrichment that could be reached is suitable for metabolomic studies in most cases. In addition to these applications to molecules of biological interest, this study reveals a rich and underestimated chemistry on the surface of RuNPs, which can be further exploited as novel reagents in organic chemistry.

In summary, simple organic polymers can be efficiently used for the organometallic synthesis of RuNPs, giving rise to the formation of very small nanoparticles (down to ca. 1 nm) which are stable under inert atmosphere. These nanoparticles can be isolated as a powder and dissolved when required. This steric stabilization is a great advantage for reactivity and mechanistic studies. A new way for catalysis and organic chemistry has recently been opened due to novel results in the regioselective and stereospecific isotopic labeling of nitrogen-containing compounds.

2.2 Alcohol-Stabilized RuNPs

Similarly to numerous data in the literature, our initial results showed that RuNPs could be stabilized in a simple polymer matrix which exhibits very weak chemical interactions with the NP surface. The next questions were: (1) how weak a stabilizer

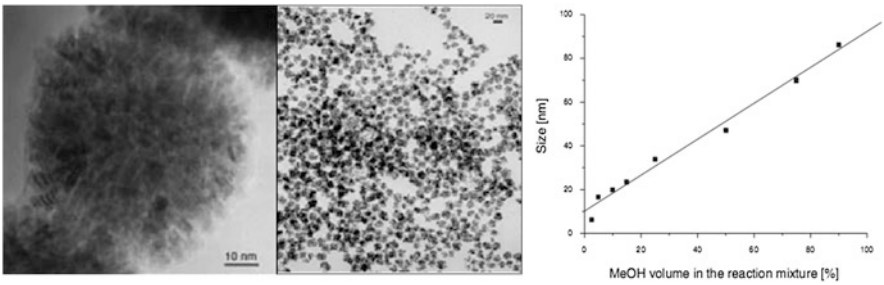

Fig. 4 Polycrystalline "spongelike" RuNPs obtained in pure methanol (*left*), in a 10/90 mixture of methanol and THF (*middle*) and linear correlation between the MeOH/THF volume ratio and the particle size (*right*). (Adapted from [64, 65] with permission from Wiley)

can be? (2) under very mild conditions, can we prepare nano-objects displaying their own stability (giant clusters)? For this purpose, the organometallic precursor [Ru(COD)(COT)] was dissolved in various solvents to then react with an H_2 atmosphere. Whilst only a black ruthenium precipitate was obtained in neat pentane, dichloromethane and THF, a stabilization was observed in some neat alcohols and THF/alcohol mixtures in the absence of further stabilizer [64, 65]. The particles were characterized by TEM, XRD, WAXS, and XPS. TEM micrographs revealed the presence of polycrystalline sponge-like particles of regular spherical shape and homogeneous size. In addition, both isolated and well-dispersed monocrystalline particles were sometimes observed depending upon the solvent mixture and the alcohol alkyl chain length (from C1 for methanol to C5 for pentanol). In all cases, size distributions were relatively narrow. WAXS and XRD analyses indicated the exclusive presence of hcp ruthenium in these materials. The size of the particles could be controlled by adjusting the reaction temperature or the composition of the solvent mixture. In pure methanol, the formation of large polycrystalline particles of 76 nm mean size was observed (Fig. 4, left). Smaller nanostructures are formed by decreasing the quantity of methanol in a MeOH/THF reaction mixture. As examples, nanostructures of mean size 16 nm were formed for a MeOH/THF/ ratio of 10/90 in volume (Fig. 4, middle) and nanostructures of a size range of 3–6 nm for a 2.5/97.5 MeOH/THF ratio. A surprising linear correlation was established between the solvent composition and the size of the particles in the range 4–85 nm (Fig. 4, right).

In addition, the particles display different spongelike morphologies depending upon the medium composition. In MeOH-rich mixtures, this spongelike aspect is more pronounced than in MeOH poor media. The colloidal solutions obtained in these reaction conditions are surprisingly very stable, i.e. they can be kept under argon for very long periods of time. The less stable solutions were prepared in MeOH-rich solutions which also contain the largest particles. The size and morphology variations observed upon changing the solvent mixtures were also unexpected. These observations were related to the increase in polarity of the solution upon adding MeOH in THF. This led us to suspect the segregation of cyclooctane,

which is synthesized from the reduction of the precursor, within the more polar solvents. In this respect, larger droplets are likely to be formed in the most polar solvent systems which are consequently expected as the most segregated medium. This hypothesis was confirmed following further experiments, i.e. adding excess of cyclooctane to a MeOH/THF 10/90 solution while keeping other parameters constant. The addition of 2 or 20 equiv. cyclooctane (equiv./initial Ru) led to an increase of the particle size of a factor 1.5 or 2, respectively. These results were consistent with the formation of ruthenium particles within the cyclooctane droplets ("nanoreactors"), i.e. the stabilization of the RuNPs in these systems results from a segregation phenomenon in the reaction mixture. Interestingly, this result implies that the nanoparticles are more soluble in cyclooctane than in alcohols. Although the origin of this phenomenon was not clear at that time, we have then demonstrated that the surface of the particles prepared in our conditions under H_2 accommodate between 1 and 2 hydrides per surface Ru atom. Since the polarity of the Ru–H bond is comparable to that of a C–H bond in molecular chemistry, these experiments suggest that the RuNPs prepared according to our procedure can be viewed as large grease bowls.

Using alcohols displaying longer alkyl chains than methanol, an important change in the nature of the particles was observed. Whilst the particles are homogeneous in size, their size drops to 2–5 nm for propanol, isopropanol, and pentanol. The particles are monocrystalline in pentanol and display a mean size of 3 nm. In *n*- and iso-propanol, the particles are slightly larger (4.8 nm in *n*-propanol) and may be polycrystalline. In all these cases, the solutions are stable (3–4 months in *n*-propanol). In pure heptanol [66], small and single crystalline RuNPs of 3 nm mean size were obtained, displaying the compact hcp structure. These NPs could be isolated as a black powder by: (1) evaporation of the solution to dryness, (2) concentration of the solution and precipitation from pentane. Microanalytical data on this powder indicated the presence of ca. 70% Ru and ca. 1 heptanol: 7.5 Ru. Considering these data and the RuNPs mean size of 3 nm, a calculation provided an estimation of 123 heptanol molecules present in the vicinity of the particles made of 923 Ru atoms (whose 362 are located on the surface). Whilst these heptanol ligands are associated with the ruthenium surface, some heptanol molecules may not be directly coordinated on this surface. However, the characterization of these purified particles by ^{1}H and ^{13}C solution NMR in THF-d^8 revealed the coordination of heptanol on their surface. Whilst the protons located on the carbon in α-position to oxygen were not visible, the protons located on the β carbon were very broad and not distinguishable from the other $–CH_2–$ of the alkyl chain. These observations were attributed to the presence of a fast exchange between free heptanol and heptanol coordinated to the surface of a large particle tumbling slowly in the solution. In addition, the presence of dihydrogen desorbing from the RuNPs surface was detected by ^{1}H NMR. This was attributed to the presence of hydrides on the RuNPs surface as a result of their synthesis conditions. All these observations were in favor of the concomitant presence of both "X" functional ligands (hydrides) and "L" labile ligands (heptanol molecules) at the RuNP surface. This suggested the possibility to develop a novel complex chemistry

using the traditional concepts of organometallic chemistry and monodisperse particles as "super-atoms." Finally, all these particles prepared in alcohols appeared extremely reactive when isolated in the solid state since they burned in contact with air. Catalytic studies performed with the nanoparticles prepared in 10% MeOH showed that these RuNPs are active for the reduction of benzene to cyclohexane in mild conditions (20 bar, 80°C, 15 h) and remain unaltered following their evaluation in catalysis.

All these results obtained with alcohols suggested the presence of hydrogen on the surface of the particles and raised the question of the nature of the stabilization mechanism of the particles prepared by hydrogenation of [Ru(COD)(COT)] in alcoholic medium. It appeared that depending on the nature of the alcohol, i.e. the length of the alkyl chain and the polarity, the control of the growth of the nanoparticles may result (1) from the size of "nanoreactors" formed in the reaction medium due to a segregation phenomenon and (2) from a weak-coordinating effect of a ligand when the alkyl chain of the alcohol is long enough.

2.3 Ligand-Stabilized RuNPs

Following our achievements with polymers and alcohols, our research widely focused on the preparation of well-defined RuNPs stabilized by ligands of different natures [67]. Some of our aims were to better understand how a ligand can affect the surface chemistry of the nanoparticles as well as how the stabilization of the nanoparticles depends on the interaction of the ligand with the metallic surface. Another interest for us in using ligands was their potential to orientate the course of a catalytic reaction by inducing selectivity, a well-known phenomenon in homogeneous catalysis. Whilst numerous efforts have been devoted to the use of simple ligands, more sophisticated molecules have also been selected for the development of nanocatalysts with improved catalytic performances in comparison with already known homogeneous and heterogeneous catalysts. Our studies to develop novel RuNP nanocatalysts mainly involved ligands containing nitrogen (amines, aminoalcohols, oxazolines), phosphorus (diphosphites, phosphines, secondary phosphine oxides), or carbon (carbenes) as coordinating atoms to the metal surface. Here, we discuss how the ligand can control different properties of the nanoparticles such as their size, shape, and surface reactivity. Some RuNPs have been applied in catalysis, mainly in hydrogenation reactions of model substrates and also in dehydrogenation of amine-boranes.

2.3.1 Amine-Stabilized RuNPs

Amines are frequently used for the synthesis of metal nanoparticles. Amines can act as reducing agent and as stabilizers due to their σ-type coordination mode to the metallic surface (see for example: [68–70]). The use of simple amines for the

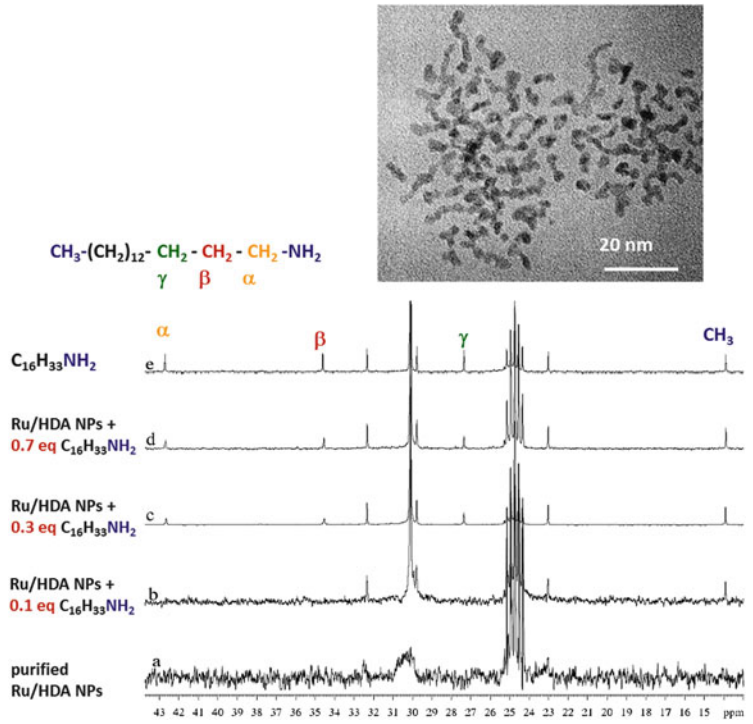

Fig. 5 TEM image of RuNPs stabilized with 0.2 equiv. of hexadecylamine (*top*) and ^{13}CNMR studies (100.71 MHz, THF–d^8, 303 K) (*bottom*): (**a**) purified colloid, (**b**) colloid + 0.1 equiv. HDA, (**c**) colloïd + 0.3 equiv. HDA, (**d**) colloid + 0.7 equiv. HDA, (**e**) pure HDA. (Adapted from [61] with permission from ACS)

stabilization of RuNPs was described by our group in 2001 [61]. The decomposition of the [Ru(COD)(COD)] complex was performed under the same reaction conditions as with polymers or alcohols (3 bar H_2, RT) but using $C_8H_{17}NH_2$, $C_{12}H_{25}NH_2$ or $C_{16}H_{33}NH_2$ (0.2, 0.5 and 1 M equiv./Ru) as stabilizers. Whilst hcp RuNPs are formed in all cases, both the nature and concentration of the ligand control the size and dispersion of the nanoparticles. For example, using 0.2 equiv. of octylamine led to the formation of superstructures of 100 nm which results from the agglomeration of isolated nanospheres with a mean size of 2.3 nm. Interestingly, higher concentrations of octylamine yields more agglomerated structures. Using hexadecyl- and dodecylamine results in the formation of nanoparticles with elongated shape, whose size is dependent upon the molar ratio Ru:L (in all cases the sizes are found between 1.8 and 2.6 nm). When the concentration of ligands in the solution is increased (Fig. 5), the nanoparticles show a tendency to agglomerate which leads to worm-like nanoparticles with a large size distribution.

Since the size and shape of the nanoparticles are not well controlled, these results demonstrate that amines do not ensure a strong stabilization of the particles. This is also consistent with the tendency of these nanoparticles to display a vermicular

aspect. This lack of control was thought to result from a weak coordination of the amine ligand to the surface of the particles via the nitrogen atom. To study the behavior of the amines, these colloids were analyzed by liquid ^{1}H and ^{13}C NMR which confirmed the coordination of the amine ligand to the surface of the nanoparticles (Fig. 5). It is worth mentioning that the signals corresponding to the carbons located in the α, β, and γ positions relative to the amino group are not observed on the NMR spectra of the RuNPs stabilized with hexadecylamine (0.2 equiv.). These peaks correspond to the carbons located in close vicinity of the metal surface which are not visible. As previously discussed for the stabilization of the nanoparticles by heptanol, this is related to a very short T_2 resulting from the slow tumbling of the particles in solution due to their large size. To shed more light on the interaction of the amine with the NP surface, extra ligand was progressively added in the NMR tube. This study demonstrated that a fast equilibrium occurs between the free amine and the amine coordinated at the NP surface at the NMR time scale. As a consequence, the coordination of the ligand at the surface of the colloids is a dynamic process which implies a weak interaction between the ligand and the metallic surface of the nanoparticles. The mobility of the amines favors the coalescence of the initial nanospheres particles. In addition, the wormlike shape may result from a self-organization of the ligands in the solution.

The ability of long alkyl chain amines to induce a shape control of ruthenium nanostructures from ruthenium complexes has been explored by other groups and significant advances have recently been described. Different protocols in organic medium leading to monodisperse nanoparticles such as stars, urchins, and hourglass, from $Ru(acac)_2$ [71] and $Ru_3(CO)_{12}$ [72], have been reported. These syntheses require the presence of an amine or a mixture of an amine plus a carboxylic acid which play a crucial role in controlling the shape of ruthenium nanocrystals

For example, Tilley and coworkers recently achieved the synthesis of ruthenium nanocrystals which can exhibit a sophisticated hourglass morphology, i.e. two truncated hexagonal pyramids connected at their vertices (Fig. 6) [71]. The hourglass nanocrystal consists of {101} facets at the sides and {001} facets at the ends while truncated corners are {101} facets. These nanocrystals were prepared in a yield of 77% from the reduction of ruthenium(II) acetylacetonate in mesitylene under hydrogen atmosphere at 140°C for 70 h in the presence of dodecylamine (DDA). They are 18 ± 3 nm in length, 11 ± 2 nm wide, and exhibit intermediate necks which are 4 ± 1 nm thick. During the synthetic process, 19% of rod-like and 4% of near-spherical nanocrystals were also synthesized. It is worth mentioning that a mixture of hourglasses and spheres can self-assemble in a binary superlattice (Fig. 6, right). Interestingly, a three-step growth process has been observed by HRTEM during the formation of the hourglass nanocrystals: (1) formation of partially crystallized rod-like nanoparticles from the coalescence of ruthenium nanoparticles to decrease their surface free energy, (2) crystallization of the rod-like nanoparticles resulting in single crystalline nanocrystals, this is possibly driven by the high strength of Ru–Ru bonds which compensates the entropic cost required to eliminate defects, (3) overgrowth leading to nanocrystals with a well-defined hourglass morphology which exposes facets of low surface energy.

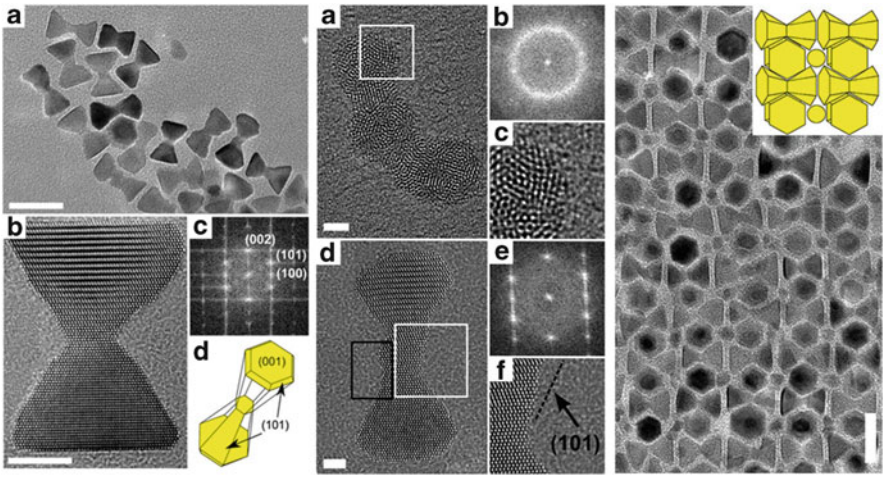

Fig. 6 *Left*: Ruthenium hourglass nanocrystals synthesized after 70 h. (**a**) TEM image of ruthenium hourglass nanocrystals, scale bar = 20 nm. (**b**) HRTEM image of a single, highly crystalline, ruthenium hourglass nanocrystal, scale bar = 5 nm. (**c**) FFT of the ruthenium hourglass nanocrystal shown in (**b**). (**d**) Schematic of a single ruthenium hourglass nanocrystal showing termination by {001} and {101} facets; *Center*: Ruthenium hourglass nanocrystal intermediates. (**a**) HRTEM image of a partially crystalline ruthenium rod-like nanocrystal intermediate isolated after 48 h, scale bar = 2 nm. (**b**) FFT of the ruthenium rod-like nanocrystal shown in (**a**). (**c**) High magnification HRTEM image of the surface of the rod-like nanocrystal as shown by the *white box* in (**a**). (**d**) HRTEM image of a single crystal ruthenium hourglass-like nanocrystal intermediate isolated after 52 h, scale bar = 2 nm. (**e**) FFT of the ruthenium hourglass-like nanocrystal shown in (**d**). (**f**) High magnification HRTEM image of the surface of the hourglass-like nanocrystal as shown by the *white box* in (**d**); *Right*: TEM image of a binary nanocrystal superlattice formed by the evaporation of a mixture of ruthenium hourglass nanocrystals and spherical ruthenium nanocrystals. Scale bar = 20 nm. (Reproduced from [71] with permission from ACS)

Lignier et al. achieved the synthesis of Ru nanostars (Fig. 7) from the decomposition of $Ru_3(CO)_{12}$ in toluene at 160°C under dihydrogen in the presence of hexadecylamine (HDA) and hexadecanoic acid (PA) [72]. Under these conditions, the nanoparticles are catalysts for both arene hydrogenation, e.g. toluene, and the Fischer–Tropsch reaction. Whilst the direction, location, and number of branches are not identical in all nanostars, the uniformity of the particle size is high, especially in view of their complex three-dimensional morphology. The metallic state and hcp structure of the Ru nanostars, which are approximately 15 nm across, were determined by XRD, X-ray photoelectron spectroscopy (XPS), and HRTEM. Following the extension of the reaction time to 24 h, the nanostar shape is preserved which reveals the stability of these branched nanocrystals.

An increase of HDA concentration led to a higher rate of nanoparticle formation from $Ru_3(CO)_{12}$, while an increase of PA concentration had the opposite effect. This is likely to be related to the presence of ruthenium–amine and ruthenium–carboxylate complexes as intermediates in the synthetic process. Before the formation of the nanostars, quasi-spherical and unbranched nanoparticles were first

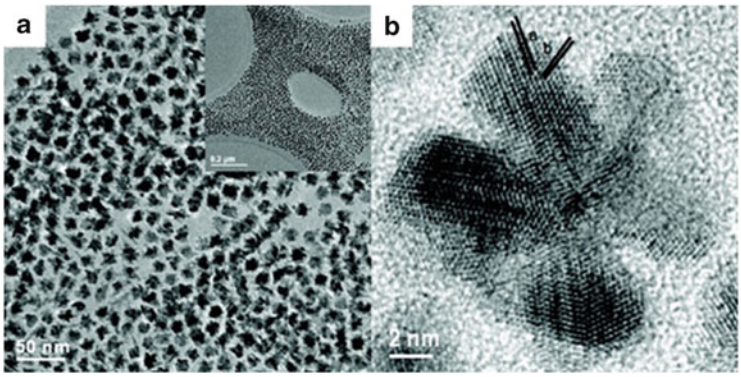

Fig. 7 (**a**) TEM images of Ru nanostar particles prepared from $Ru_3(CO)_{12}$ with a 1:3 ratio of PA/HAD at 160°C for 6 h. (**b**) HRTEM image of a typical Ru nanostar. The *d*-spacings of parts (**a**) and (**b**) are 0.21 and 0.20 nm, respectively, and can be indexed to the (002) and (101) planes of hexagonal ruthenium. Twin defects and stacking faults are clearly present. (Reproduced from [72] with permission from ACS)

obtained. No discernible grain boundaries were present in these polycrystalline nanoparticles which constitute the core of nanostars. Then, the formed branches are single crystalline or exhibit twin defects and stacking faults. These defects, which are parallel to the crystal growth direction, result from the propagation of the defects during the growth of the branches. This reveals that the growth of the branches proceeds by addition of monomer from solution and not by oriented attachment or agglomeration of smaller nanoparticles. Since the nucleation and growth of the branches occur on the cores, the size uniformity of the nanostars is related to the monodispersity of the cores. In addition, the location of the branches results from both the morphology and crystallinity of these cores. Unexpectedly, a novel crystallization step occurs in the nanostar formation since single crystalline nanostars are formed from polycrystalline seeds.

Interestingly, a dramatic increase in the length of the branches is obtained following the additional injection of ruthenium precursor in the solution containing the nanostars, i.e. by seeded growth. This results in the formation of monodisperse nanourchins (Fig. 8). A molar ratio of acid/amine/Ru of 1/2/1 is required to achieve the slow decomposition of the metal precursor which favors heterogeneous nucleation. Similarly to the nanostars, the controlled addition of monomers results in the formation of the branches which are single crystalline or exhibit defects oriented in the direction of the growth.

In summary, simple amines are weakly coordinated ligands which are not appropriate for the synthesis of small spherical RuNPs in our reaction conditions. Nevertheless, interesting worm-like shapes were observed. In addition, the presence of amines allows the growth of preformed nuclei, which suggest the potential of amines for a shape-controlled synthesis of MNPs. This advantage was confirmed by results from other groups which reported sophisticated nanostructures displaying

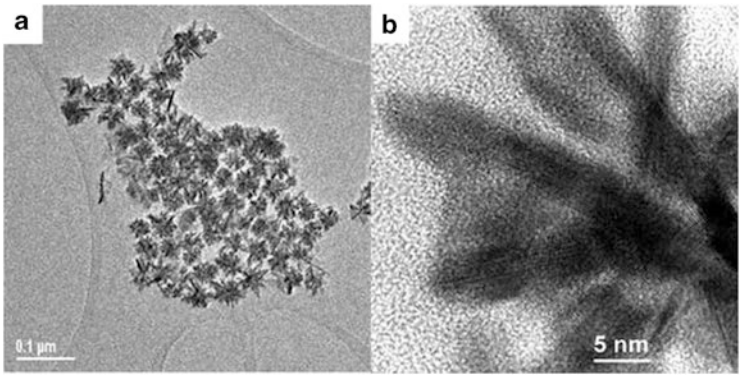

Fig. 8 (**a**) TEM and (**b**) HRTEM images of Ru nanourchins prepared from Ru nanostars by adding $Ru_3(CO)_{12}$ with a 1:2 ratio of PA/HDA at 160°C. (Reproduced from [72] with permission from ACS)

well-defined crystalline faces. As a consequence, these novel nano-objects are of high interest for catalysis as they may induce a different selectivity.

2.3.2 Diphosphine-Stabilized RuNPs

It is well known from molecular chemistry that phosphine ligands are usually strong σ-donor ligands and only weak π-acceptors. Interestingly, this effect can be increased by the presence of electron-donating substituents. In addition, the size and steric hindrance of the phosphine ligands is approximately described by the cone-angle (θ) of the phosphine. In the field of metal nanoparticles, the phosphines are not often used as stabilizers. From our experience, the use of phosphine gave rise to a very efficient stabilization of the RuNPs which are generally well defined with a spherical shape and a small size. By playing with the susbtituents on the phosphorus atom, it was possible to tune the surface properties of RuNPs and the related catalytic reactivity of this surface.

Since polyphosphines were efficient ligands for the synthesis of PdNPs [73], a similar methodology was applied to RuNPs. As discussed in the introduction, this metal presents a lower Knight-shift than Pt and Pd. This facilitates the characterization of the surface state of the particles using NMR. For that purpose, the study was focused on simple diphosphines, i.e. 1,4-bis(diphenylphosphino)butane (dppb) and 1,10-bis(diphenylphosphino)decane (dppd) [74]. The nanoparticles were prepared from [Ru(COD)(COT)] in the presence of 0.1 equiv. of the corresponding diphosphine (the diphosphine/Ru ratio was optimized to add the lower quantity of ligand as possible; it gives rise to 0.2 equiv. of P/Ru), in THF under 3 bar of dihydrogen at RT. This resulted in the formation of stable, crystalline, and monodisperse hcp nanoparticles which exhibit a mean size of 1.5 (dppb) and 1.9 nm (dppd). The presence of the ligand at the surface of the NPs was confirmed by

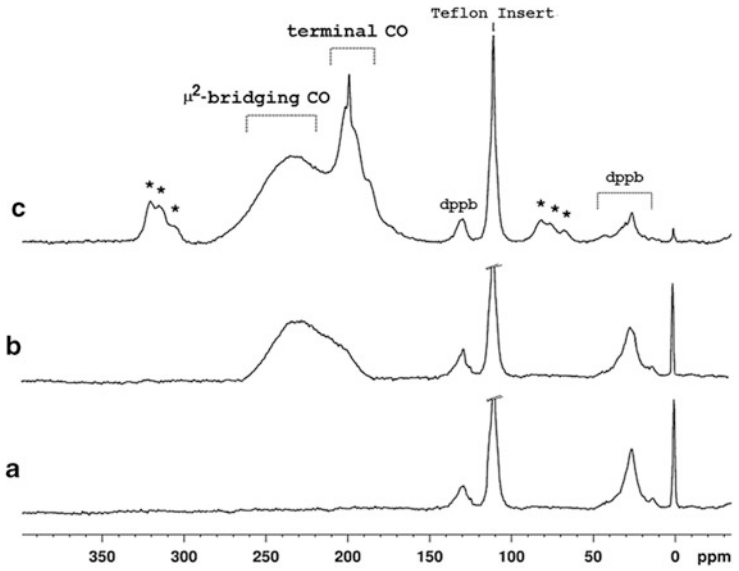

Fig. 9 ^{13}C MAS NMR spectra of dppb-stabilized RuNPs after adsorption of ^{13}CO: 0 h (**a**), 2 h (**b**), 12 h (**c**), (*asterisk*: spinning side-band). (Reproduced from [75] with permission from Wiley)

solution ^{31}P NMR following the treatment of the NPs with H_2O_2 to release the oxidized phosphine. This result was also confirmed by MAS ^{31}P NMR. The quantification of the hydrides present at the surface of the Ru/dppd particles was performed by titration with an olefin, leading to a reproducible value of 1.1 hydrides by surface ruthenium atom. This value is lower than for HDA or PVP ligands since 1.3 hydrides by surface ruthenium atom were measured for both Ru/HDA and Ru/PVP.

The surface state of the dppb-stabilized RuNPs was investigated using ^{13}CO as a probe molecule via IR and MAS NMR techniques [62]. These studies demonstrated that, in contrast to the case of ^{13}CO adsorbed on Ru/PVP NPs, the CO ligands are not fluxional. This is related to the presence of the ancillary phosphines ligands at the surface of the RuNPs (Fig. 9). In addition, the presence of bridging terminal and multicarbonyl group was evidenced. Unexpectedly, similar studies carried out with labeled ethylene demonstrated the breaking of the C–C bond to produce methyl groups firmly attached to the surface [74].

In continuity of this study, the reactivity of dppb and PVP-stabilized RuNPs was compared using standard reactions, i.e. CO oxidation, CO_2 reduction and styrene hydrogenation [75]. The aim of the work was: (1) to study the effect of ligands on the intrinsic reactivity of metal nanoparticles and (2) to identify the sites of reactivity on the nanoparticles by using NMR and IR spectroscopies. Through simple experiments, it was demonstrated that CO oxidation proceeds at RT on RuNPs. However, a rapid deactivation of this system occurred in the absence of ligands (RuPVP NPs) because of the formation of RuO_2. In the presence of dppb

ligands, the reaction involved exclusively the bridging CO groups and no bulk oxidation was observed at RT under catalytic conditions. The reverse reaction, CO_2 reduction, was achieved at 120°C in the presence of H_2 and led to CO, which coordinated exclusively in a bridging mode. This demonstrates the competition between hydrides and CO for the coordination on RuNPs. The effect of ligands localized on the surface was also evidenced in catalytic reactions. In Ru/PVP and Ru/dppb systems, styrene is slowly hydrogenated at RT: first into ethylbenzene and then into ethylcyclohexane. Whilst the selective poisoning of the nanoparticles with bridging CO groups led to catalysts only able to reduce the vinyl group of styrene, a full poisoning of the surface with both terminal and bridging CO groups led to inactive catalysts. These results evidenced that bridging CO groups and arenes compete for the same sites on the surface of the particles. This also suggested that the sites accommodating both arenes and bridging CO groups are present on the faces. In addition, this work showed that: (1) diphosphine ligands are located in the proximity of terminal CO groups, (2) hydrides can selectively displace the terminal CO groups and not the bridging ones. About CO oxidation and arene reduction, the selectivity could be related to the availability of the faces. While it was expected that arene hydrogenation occurs on compact faces, the necessity of bridging groups for CO oxidation was not obvious.

Diphosphine ligands strongly coordinate at the surface of RuNPs forming a system of choice to compare the surface properties of polymer- and ligand-stabilized RuNPs. CO oxidation, CO_2 reduction, and styrene hydrogenation provided a picture of small RuNPs at the molecular level: (1) CO preferably binds in a bridging mode on face atoms which are also the sites for the hydrogenation of arenes. These face atoms are also the preferred sites for CO oxidation. (2) Hydrides and terminal CO compete for sites located near the bulky diphosphine ligands. These sites are likely to be apexes and edges since they are inactive for arene hydrogenation.

2.3.3 Phenyl Pyridine-Stabilized RuNPs

In a collaborative work with Gomez et al. we reported the synthesis of RuNPs using the 4-(3-phenylpropyl)pyridine (PPy) as a stabilizing ligand [76]. This unusual ligand was selected due to its simple structure containing a pyridine group, which can favor the approach of the flat phenyl to the metallic surface upon σ-coordination. As a consequence, this ligand was relevant to elucidate π-interactions between the ligand and the metallic surface. In fact, previous investigations of the Heck coupling reactions with PdNPs showed that a phenyl group is required in the ligand or the substrate [77, 78]. RuNPs were prepared via the decomposition of [Ru(COD)(COT)] under dihydrogen in the presence of PPy (0.2 M equiv./Ru). Optimized conditions led to reproducible NP syntheses, giving rise to small nanoparticles with a mean diameter of 1.3 ± 0.3 nm (Fig. 10).

Whilst this result contrasted with our synthesis of large and agglomerated particles using simple pyridines as stabilizers, this was consistent with previous

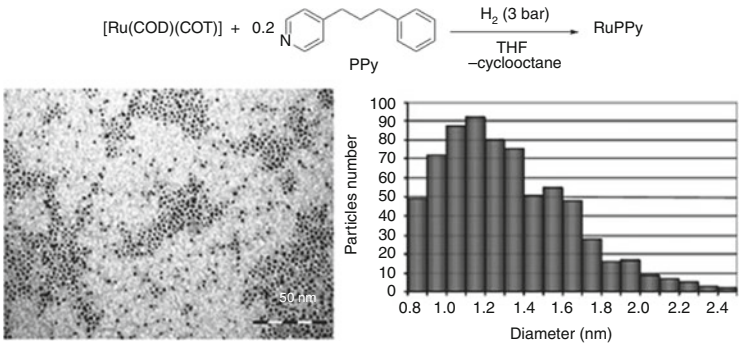

Fig. 10 Synthesis, TEM image and size histogram for RuNPs stabilized with 4-(3-phenylpropyl) pyridine (PPy). (Adapted from [76] with permission from RSC)

reports on gold particles using pyridine [79]. The coordination of the PPy ligand to the ruthenium surface was attested by ^{13}C CP-MAS NMR. Narrow aliphatic peaks and a broad signal in the aromatic region showed that an aromatic group in PPy participates to the stabilization of the particles. In addition, this favors their dispersion probably as a result of the coordination of the phenyl group on the metallic surface. Following the treatment of RuNPs under deuterium atmosphere, ^{2}H MAS NMR experiments revealed the presence of two signals: one attributed to Ru–D bonds and one attributed to C–D bonds with a 120 kHz quadrupolar splitting, which is consistent with previously reported data [80]. This evidenced the presence of organic stabilizers on the RuNPs surface which are able to exchange their hydrogen with surface deuterides. Finally, a quantitative release of unreduced PPy could be achieved after 24 h of reaction, showing both the effective presence of the ligand at the surface of the particles and the strong interaction of this ligand with the metallic surface. The ligand coordination to RuNPs was studied by ^{1}H NMR under the conditions of the NP preparation. This technique enabled us to follow the decomposition of the ruthenium complex as well as the evolution of the ligand once coordinated at the surface of the particles. This allowed us to observe that the signal broadening was faster for the *ortho*-pyridinyl protons than for the aromatic protons. This can be related to the interaction of the ligand with the metallic surface, first via the nitrogen atom of pyridinyl group and then via a π-interaction, which is consistent with the absence of Ru-N absorption band in the IR spectrum.

These RuPPy NPs appeared to us as a model of choice to develop surface reactivity studies based on NMR. This approach was expected to improve our understanding of mechanistic aspects of hydrogenation reactions catalyzed by RuNPs [80]. For that purpose, the surface reactivity of the RuPPyNPs was explored with various aromatic substrates using different NMR experiments. First, the high stability of RuPPy NPs has been demonstrated in the presence of several aromatic substrates during hydrogenation studies. The hydrides present on the surface reacted selectively with the vinyl functions of substituted arenes, the aromatic

group being not hydrogenated. No hydride transfer from the metallic surface to aromatic rings agrees with a high coverage of the metallic surface by PPy molecules. Mechanistic studies by NOE NMR experiments using proton selective excitations evidenced the coordination of the pyridine derivatives (4-(3-phenylpropyl)pyridine, 4-vinyl-pyridine and 4-ethyl-pyridine) in contrast to styrene and ethylbenzene. Since the magnetization exchanges are faster than residential times on the metallic surface at the NMR time scale of the experiences, intermolecular NOE effects were observed between 4-vinylpyridine and 4-ethylpyridine. In the presence of an excess of dihydrogen, all substituted aromatic substrates were hydrogenated under mild conditions, probably through transient displacement of the coordinated phenyl ring.

In summary, 4-(3-phenylpropyl)-pyridine efficiently stabilizes very small RuNPs. A precise analysis of the behavior of RuPPyNPs in solution by NMR investigations revealed that 4-(3-phenylpropyl)pyridine acts as a "bidentate" ligand which is strongly coordinated to the metallic surface through π,π-interaction. This can be considered as a novel and specific mode of coordination on the nanoparticle surface although such π-coordination has previously been proposed, e.g. for the coordination of cinchonidine on Pt nanoparticles. In addition, this study demonstrated the potential of specific ligands, such as PPy, to efficiently stabilize the nanoparticles while preserving their reactivity.

2.3.4 Carbene-stabilized RuNPs

Since the achievements of Grubbs on metathesis, N-heterocyclic carbene ligands (NHCs) are strongly related to ruthenium in molecular chemistry. However, these ligands had not been used for the stabilization of ruthenium nanoparticles despite the work of Tilley et al. on AuNPs [81]. It was therefore of interest, following a comprehensive study of phosphine coordination on nanoparticles, to investigate the interaction between RuNPs and NHCs [82]. The ruthenium nanoparticles were prepared by decomposition of [Ru(COD)(COT)] in pentane (3 bar H_2; RT) in the presence of a carbene, i.e. 1,3-bis(2,6-diisopropylphenyl)imidazol-2-ylidene (IPr) or *N*,*N*-di(*tert*-butyl)imidazol-2-ylidene (I^{t}Bu), as shown in Fig. 11.

Different colloids were obtained depending on the amount and the type of carbene. Whilst RuNPs with a mean size of 1.7 nm were formed using 0.2 equiv. of IPr or 0.5 equiv. of I^{t}Bu, the mean diameter of the RuNPs is 1.5 nm using 0.5 equiv. of IPr. In all these cases, the Ru/NHC NPs are homogeneous in size and shape. In addition, WAXS analysis demonstrated that these NPs present the expected hcp structure. Since it was not possible to displace the carbene ligand at the surface of the nanoparticles in the presence of thiol, amine, or phosphine ligands, the carbenes are strongly attached to the metal surface. With the aim to study the coordination of the carbenes by IR and NMR spectroscopies, the synthesis of the RuNPs has been performed using NHCs ligands which are ^{13}C labeled in the carbene position. By this way, MAS NMR analysis (Fig. 11) allows us to detect the signals of the bonded carbene to the Ru surface in the 195–205 ppm range

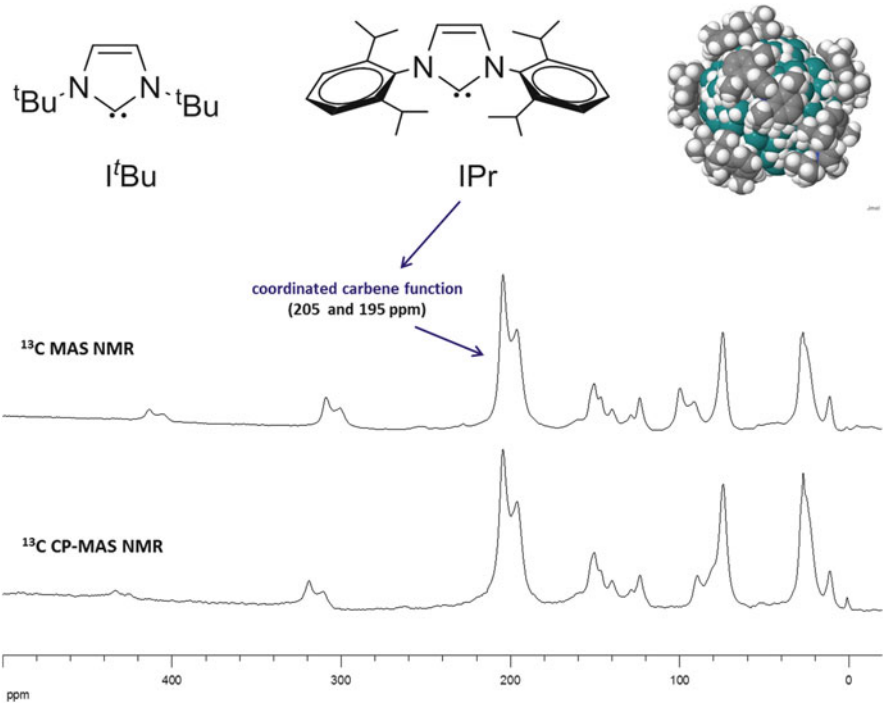

Fig. 11 *Top Left*: NHCs employed to stabilize RuNPs (*left*); *Right*: Space filling model of a 1.8 nm *hcp* RuNP stabilized by 8 IPr NHC ligands and accommodating 1.5 hydrides per surface Ru (*right*); *Bottom*: ^{13}C MAS and CP-MAS NMR spectra of RuNPs/*i*Pr* ([*i*Pr*]/[Ru]$_0$ =0,5). (Adapted from [82] with permission from Wiley)

(depending on the type and amount of carbene used). Carbon monoxide was used to probe the sites available at the surface of the NHC-stabilized RuNPs since it was expected that CO resonances would inform us on the coordination of the carbenes. For the nanoparticles prepared with 0.5 equiv. of I^{t}Bu, the CO is predominantly present in bridging mode. Whilst this coordination mode is also observed when CO is added to the colloid prepared with 0.2 equiv. of IPr, the colloids prepared using 0.5 equiv. of IPr only exhibit linear and multicarbonyl adsorption (i.e. no bridging CO). From these results, the location of the different carbene ligands at the surface of the RuNPs can be proposed. For the nanoparticles prepared using 0.5 equiv. of I^{t}Bu or 0.2 equiv. of IPr, CO is located on the faces while the ligand is located on edges and apexes. In contrast, for the RuNPs prepared with 0.5 equiv. of IPr, the absence of bridging CO is in agreement with the full coverage of the nanoparticle surface by the IPr ligand. These carbene-stabilized RuNPs showed a moderate activity in the hydrogenation of styrene under mild conditions. As expected for RuNPs, the hydrogenation of the vinyl bond is followed by the hydrogenation of the aromatic ring. In collaboration with P. van Leeuwen *and coworkers*, these NHC-stabilized RuNPs were used as catalysts in the hydrogenation of different

substrates (benzene derivatives, methylanisoles, acetophenone) under various reaction conditions (solvent, substrate concentration, substrate/metal ratio, temperature) [83]. The Ru/NHC NPs appeared as active catalysts in the hydrogenation of aromatics and showed an interesting ligand effect, i.e. Ru/IPr NPs were generally more active than Ru/I^{t}Bu NPs.

In summary, carbene ligands, known to be excellent ligands for molecular Ru complexes, are equally efficient for the stabilization of RuNPs. The strong binding of the NHC ligands to the surface was evidenced by NMR via ^{13}C labeling of the carbenes and addition of ^{13}CO. In addition, we were able to identify the probable location of these NHC ligands on the nanoparticles (Fig. 11 right). Finally, we demonstrated that the substituents of the carbenes influence the reactivity of the nanoparticles which is mainly due to steric effects.

2.4 Bimetallic RuPt, RuFe, and RuSn NPs

Bimetallic NPs are emerging as an important class of material offering a vast number of possible structures and compositions. As a consequence, these materials are expected to exhibit superior performances and even novel properties [84]. Usually, bimetallic NPs are classified on the basis of the chemical distribution of the two metals in the NPs. One can distinguish (1) bimetallic alloys characterized by the formation of a statistical distribution of the two elements and (2) bimetallic heterodimers or core-shell nanostructures in which monometallic domains are segregated. The NPs can exhibit synergetic effects resulting from the intimate contact between the two metals, or can fulfil multifunctional tasks due to the association of two metal domains with different properties. This diversity of structure raises issues about the control of the chemical order in bimetallic NPs [85–87]. First, perfect bimetallic alloys require comparable kinetics of decomposition of the precursors. However, as reported by Bradley et al. [88], surface chemistry has also a huge impact on the final distribution of each metal in the NPs. As a consequence, molecular chemistry appears as a powerful tool to engineer the synthesis of complex nano-objects as illustrated by the synthesis of various alloys in our group including Ru-based bimetallic nanostructures, e.g. RuPt [89–92], RuFe [93] and RuSn [94].

Varying the kinetics of decomposition of the precursors was profitable for the controlled synthesis of RuPt NPs. Whilst the co-decomposition of [Ru(COD(COT)] and [Pt(dba)$_2$] in the presence of polyvinylpyrrolidone as stabilizer led to a RuPt alloy with a *fcc* structure, core-shell RuPt NPs were obtained in PVP, using [Pt(CH$_3$)$_2$(COD)] (i.e., [dimethyl(1,5-cyclooctadiene) platinum (II)]) instead of [Pt(dba)$_2$] [91]. This is related to the slower rate of decomposition of [Pt(CH$_3$)$_2$(COD)]. In summary, the chemical order can be controlled via the choice of the precursor. The chemical segregation leading to core-shell RuPt results from kinetic (decomposition rate of the metal precursors) and thermodynamic (preferred location of each metal in the particle) parameters as well as from the steric

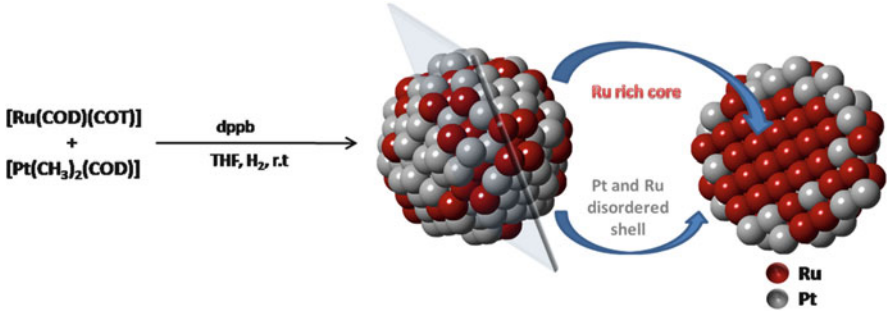

Fig. 12 Schematic representation of RuPt nanostructures synthesized from [Ru(COD)(COT)] and [$Pt(CH_3)_2$(COD)] and stabilized by diphenylphosphinobutane ligand. (Reproduced from [92] with permission from RSC)

properties of the polymer, taking into account that PVP has little or no chemical interaction with metals. In addition, it is worth mentioning the influence of the electronic properties of a diphosphine ligand on the size and chemical composition of RuPtNPs [92]. Using a strongly coordinating ligand (diphenylphosphinobutane; dppb) instead of a neutral stabilizer while keeping the same metal sources (i.e., [Ru(COD)(COT)] and [$Pt(CH_3)_2$(COD)]) and reaction conditions), nanostructures display a ruthenium-rich core and a disordered shell containing both ruthenium and platinum (Fig. 12). The complexity observed in the structure of these NPs arises from the high chemical affinity of the diphosphine ligand for both metals. These results show how a simple ligand, such as a diphosphine, can add a significant degree of complexity since the ligand significantly affects the chemical order of these bimetallic nanoparticles.

Associating a platinum metal displaying good catalytic properties, such as Ru, with a metal displaying much poorer catalytic properties may be of interest for controlling the selectivity of a catalytic reaction when several functions are accessible. In this respect, ultrasmall FeRu bimetallic nanoparticles (NPs) were prepared by the co-decomposition of two organometallic precursors, $\{Fe[N(Si(CH_3)_3)_2]_2\}_2$ and Ru(COD)(COT), under dihydrogen at 150°C in mesitylene [93]. A series of FeRu NPs of sizes of ca. 1.8 nm, which exhibit different ratios of iron to ruthenium, were obtained by varying the added quantity of ruthenium complex (FeRu : 1/1, 1/0.5, 1/0.2 and 1/0.1). The surface of the particles was shown by titration to contain ca. 0.5 hydride by surface metal atom. In addition, IR spectroscopy after CO adsorption evidenced the presence of both Fe and Ru at the surface of the particles. These FeRu NPs were used as catalyst for the hydrogenation of styrene and 2-butanone. The results indicated that the selectivity of the NPs catalysts can be modulated according to their composition. For example, whereas, in contrast to Ru NPs, Fe NPs are inactive for ketone and arene reduction in mild conditions, bimetallic NPs of composition Fe:Ru = 1:0.2 can efficiently reduce olefins and ketones but preserve the aromatic rings. This result therefore represents a case

study which demonstrates the possibility of fine-tuning the reactivity of nanocatalysts and adjusting their selectivity for a given reaction.

In another study aiming at selectively poisoning the surface of the RuNps for modulating their reactivity, tributyltin hydride [$(n\text{-}C_4H_9)_3SnH$] was added in a solution of preformed RuNPs stabilized by either a polymer (polyvinylpyrrolidone; Ru/PVP) or a ligand (bisdiphenylphosphinobutane; Ru/dppb) [94]. The idea was to take advantage of the presence of hydrides at the metallic surface to perform a simple organometallic reaction with the tin complex at the surface of the RuNPs. By this way, we could obtain tin-decorated ruthenium nanoparticles with a mean size similar to that of the preformed RuNPs. Different Sn/Ru molar ratio enabled us to study the influence of the surface tin content on the properties of these new nanoparticles and to compare them with Ru/PVP and Ru/dppb systems. In addition to HREM, WAXS, IR, NMR and Mössbauer studies, theoretical calculations and a model catalytic reaction (styrene hydrogenation) allowed us to evidence the formation of μ^3-bridging "SnR" groups on the ruthenium surface as well as to rationalize their influence on surface chemistry and catalytic activity. Whilst in the case of dppb-stabilized RuNPs, the reaction with the tin precursor was limited by the surface coverage induced by the coordination of the bulky diphosphine ligand, it was possible to vary the amount of tin deposited on the Ru surface using PVP instead of dppb. The resulting modification of the ruthenium surface led to a tuning of the surface properties of the particles, as observed through the coordination of CO as well as the catalytic hydrogenation of styrene. Ru/PVP/Sn cannot accommodate CO after the addition of even a very small amount of tin while Ru/dppb/Sn can still accommodate terminal CO groups. In addition, the Ru/PVP/Sn NPs showed a gradual variation of selectivity with increasing tin loading while only a small quantity of tin was sufficient to impede the arene hydrogenation ability of Ru/dppb NPs. These results evidence that the presence of tin adatoms on the metallic surface block some reactive sites. This approach may be a way to tune selectivity in hydrogenation reactions.

In summary, the organometallic approach is also efficient to prepare bimetallic nanoparticles. By precisely selecting the reaction conditions (precursor, stabilizer, reactant), we could access to ruthenium-based bimetallic nanoparticles displaying a controlled chemical order, i.e. alloy, core-shell, or even nanoparticles decorated with a second metal such as platinum, iron, or tin. These nanoparticles, which display different surface properties, can pave the way towards synergetic and selective catalytic performances.

3 Investigation of RuNPs in Organic Colloidal Catalysis

To pursue our work on ruthenium nanoparticles, we have investigated their surface reactivity in colloidal catalysis via the hydrogenation of model substrates. In addition, RuNPs showed promising performances for the dehydrogenation of

amine-borane in comparison with previously known homogeneous and colloidal systems.

3.1 β-Aminoalcohols and Oxazoline-Stabilized RuNPs

Asymmetric catalysis involving nanoparticles remains an important challenge since only a few examples of efficient heterogeneous catalysts have been reported [95]. With Gomez et al., we evaluated chiral β-amino alcohols and oxazolines for the stabilization of RuNPs and their applications as catalysts in the hydrogenation of unsaturated substrates [96]. The nanoparticles were prepared by decomposing [Ru(COD)(COD)] (3 bar H_2; RT) in the presence of 0.2 M equiv. of the chosen ligand. In all cases, the nanoparticles appeared stable in solution under argon atmosphere. 2-aminobutanol led to nearly spherical monodisperse RuNPs of 2.5 nm which exhibit a strong tendency to self-assemble. Amino(oxazolines) led to anisotropic RuNPs with a mean size of 2.5 nm which tend to agglomerate. The use of hydroxyl(oxazoline) yielded to well-dispersed and slightly elongated nanoparticles of 2.7 nm). Finally, well-defined nanoparticles of very small mean size (1.6 nm) and isotropic shape were obtained with bis(oxazoline) ligands. These nanoparticles are crystalline as determined by WAXS and show a tendency to aggregate into large and regular mesoscopic superstructures which result from the coordination of the ligand to different nanoparticles. NMR spectroscopy showed the coordination of the oxazoline ligands to the metal surface using methodologies previously developed to study the dynamic exchange of the amine ligand on the ruthenium surface. In addition, some dihydrogen, released in the solution, was detected, as similarly observed for ruthenium colloids stabilized with heptanol [66] or hexadecylamine [61]. This suggested that nanoparticles contain mobile hydrides at their surface. Using isopropanol as hydrogen source for the transfer of hydrogen to acetophenone, the catalytic behavior of these RuNPs was compared to Ru molecular complexes prepared in situ with the same ligands. Depending on the stabilizing ligand, the particles showed moderate to high activities. In all these cases, the formation of the *trans*-product was observed. Only Ru/amino(oxazoline) colloidal system gave asymmetric induction with a modest value of ca. 10% enantiomeric excess (ee). This very low but reproducible asymmetric induction confirmed the fluxional behavior of the amino(oxazoline) ligands at the surface of RuNPs, as previously described for Ru/amine colloids.

3.2 Diphosphite-Stabilized RuNPs

Following previous studies with diphosphite-stabilized PdNPs which led to interesting and intriguing results in Heck-coupling reactions [77, 78], the synthesis of RuNPs using carbohydrate-based diphosphites was carried out for their application

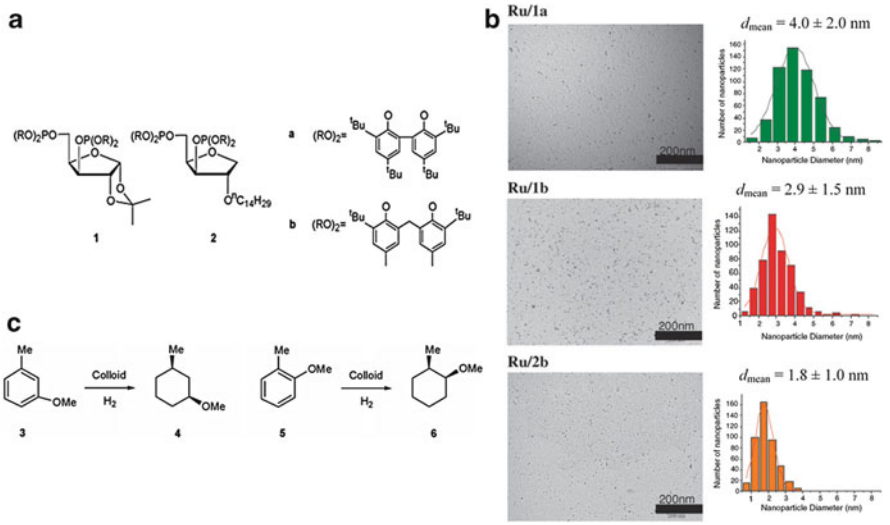

Fig. 13 (**a**) Carbohydrate-based diphosphites used for the synthesis of the RuNPs, (**b**) TEM images, and (**c**) catalytic hydrogenation of *o*- and *m*-methylanisoles with RuNPs. (Adapted from [97] with permission from RSC)

as catalysts in the hydrogenation of anisole derivatives [97]. This study was performed in collaboration with the groups of Roucoux, Claver and Castillon et al. The RuNPs were prepared as usual from [Ru(COD)(COD)] and a ligand/Ru ratio of 1:0.1 was selected, as previously used with diphosphines. Different diphosphite ligands (Fig. 13a) were employed with the objective to analyze the influence of their structure on the characteristics of the nanoparticles as well as on their catalytic activity. The question was: are such ligands adapted to induce asymmetric catalysis at the surface of the nanoparticles? TEM analysis showed the formation of RuNPs of mean size between 1.8 and 4 nm, depending on the diphosphite, thus demonstrating the influence of the ligand on the size of the particles (Fig. 13b). The smallest RuNPs were prepared in the presence of ligands which exhibit a long liphophilic chain on the sugar part or one carbon atom between the aromatic rings of the diol part.

These particles were evaluated as nanocatalysts in the hydrogenation of *o*- and *m*- methyl anisoles (Fig. 13c). As the result of a competition between the substrate and a coordinating solvent at the surface of the NPs, no conversion was observed using THF and CH_3CN as solvents for the reaction. In pentane, the particles were active and this activity was related to the nature of the ligand. The best activity was reported for the most flexible ligand which contains one carbon between the aromatic rings. The introduction of a long liphophilic chain in the ligand increased further the activity of the particles which is related to the smaller mean size and higher solubility of the nanoparticles in pentane. Contrary to the results previously obtained with aminooxazoline-stabilized RuNPs, the hydrogenation of *o*-methyl anisole gave a total selectivity for the *cis*-product. This opposite selectivity shows

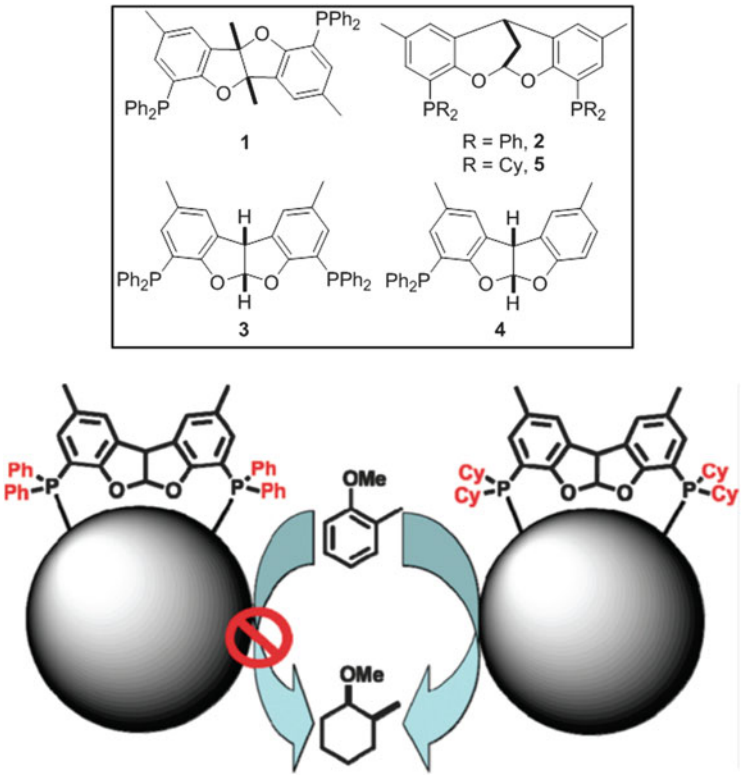

Fig. 14 Phosphine ligands used as stabilizers for the RuNPs (*top*) and difference in reactivity during hydrogenation *o*-methylanisol (*bottom*). (Adapted from [98] with permission from ACS)

that the ligand can induce different reactivities. No significant enantioselectivity was observed with diphosphites; this is probably related to the sterical hindrance of these ligands which restricts the approach of the substrate near the metal surface.

3.3 Diphosphine-Stabilized RuNPs

In nanocatalysis, an important issue is to determine whether and how ancillary phosphine ligands may influence the reactivity of the nanoparticles. In this respect, in collaboration with the group of Van Leeuwen, we investigated the design of new roof-shape phosphine ligands for the stabilization of RuNPs and their application as catalysts for the hydrogenation of aromatics [98]. The particles were prepared as usual by hydrogen-assisted decomposition of [Ru(COD)(COT)] in THF in the presence of various mono or diphosphines (Fig. 14, top) at different L/M ratios. In all cases, the prepared RuNPs have a mean size in the 1.1–2.1 nm range. Whilst

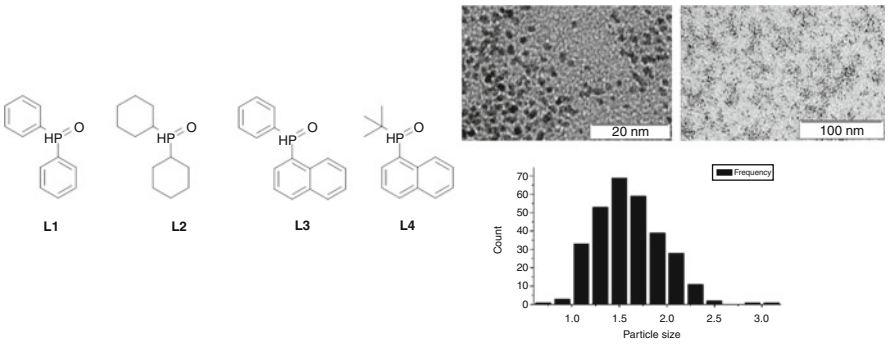

Fig. 15 Secondary phosphine oxide (SPO) used as stabilizers for the RuNPs (*left*) and TEM images of RuNPs and particle size distribution obtained with ligand L1. (Adapted from [102] with permission from RSC)

^{31}P-HRMAS NMR evidenced the coordination of the triarylphosphines, dialkylphosphines, or trialkylphosphines ligands at the surface of the particles, this also indicated the partial or total hydrogenation of the substituents due to the presence of hydrogen for the synthesis of the particles. This phenomenon was previously observed with simple diphosphine ligands [74]. The resulting nanoparticles were active in the hydrogenation of *o*-methylanisol. The nature of the ligands strongly influences the catalytic performances of these nanoparticles. It was observed that colloids containing triarylphosphines were not or very poorly active, while colloids containing dialkylarylphosphines led to the full hydrogenation of the substrate (Fig. 14, bottom). This work pointed out the interest of designing appropriate ligands to control the catalytic properties of the particles.

3.4 Secondary Phosphine Oxide (SPO)-Stabilized RuNPs

Whilst it is well established that secondary phosphine oxides (SPOs) form very strong complexes of coordination, it has been recently reported that SPOs can be efficient pre-ligands for catalytic applications [99–101]. Depending on the solvent, substituents and metal coordination, these SPOs compounds are in equilibrium which could lead to the pentavalent phosphorus oxide pre-ligand and the trivalent phosphinous acid ligand. In collaboration with van Leeuwen et al., SPO were used as ligands to prepare RuNPs (Fig. 15) [102]. These easily accessible ligands allowed the formation of air-stable small nanoparticles in the size range of 1–2 nm. The characterization of these particles employing FT-IR, liquid and solid-state NMR techniques led to insights into the structure and dynamics of surface species.

In the case of SPO ligand L1, the RuNPs were further tested for the hydrogenation of model substrates (Table 1) in acidic or basic conditions using different

Table 1 RuL1 NPs as catalysts for hydrogenation of aromatics. (Reproduced from [102] with permission from RSC)

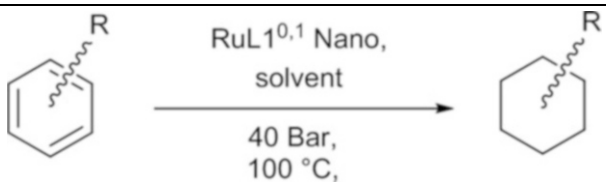

Substrate	S/C[a]	Time	Solvent	Conversion	TOF[b]
Toluene	2,400	16	THF	83	124
Cyclohexene	2,400	16	THF	100	150
Benzene	2,400	16	THF	100	150
Acetophenone	2,400	16	THF	87	130
Toluene	13,500	16	None	89	750
Toluene	13,500	6	None	59	1,330
Benzene	16,200	6	None	100	2,700
Anisole	13,300	6	None	16	350
Acetophenone	12,300	6	None	56	1,150
1,1,1-Trifluorotoluene	11,800	6	None	35	690

[a]Substrate/catalyst molar ratio. Catalyst: 1 mg of Ru-L1$^{0.1}$. 25 mL Berghof reactor connected with a 300 mL reservoir of 40 bar H_2

[b]Average turnover frequency calculated relative to hydrogenated products. TOF = mol substrate converted*mol catalyst^{-1} h^{-1}. Rate calculated by conversion not gas uptake

solvents. In homogeneous SPOs catalysis, acids and bases usually play an important role. The absence of such an effect for Ru/L1 NPs indicated that the oxygen atom is not involved in the reactions with H_2 using these nanocatalysts. The particles were highly active for the hydrogenation of aromatics with the highest hydrogenation rates achieved utilizing neat reagents (TOFs up to 2,700 mol h^{-1}). This method could be used with very low catalyst loadings (i.e., <0.01 mol% of nanoparticles) and no further additives. This work is a proof of concept that secondary phosphine oxides can be successfully used as strong ligands for nanoparticle stabilization.

3.5 APTS-Stabilized RuNPs for Dehydrogenation Reactions of Amine-Boranes

In the field of the materials for the storage of hydrogen, amine-boranes are interesting candidates due to their high hydrogen contents (19.6 wt.%) [103]. In a collaborative work with Zahmakiran and Ozkar et al., we prepared 3-aminopropyltriethoxysilane-stabilized Ru nanoclusters (Ru/APTS) of different sizes. The mean size of Ru/APTS NPs decreased with increasing APTS ligand concentration in the

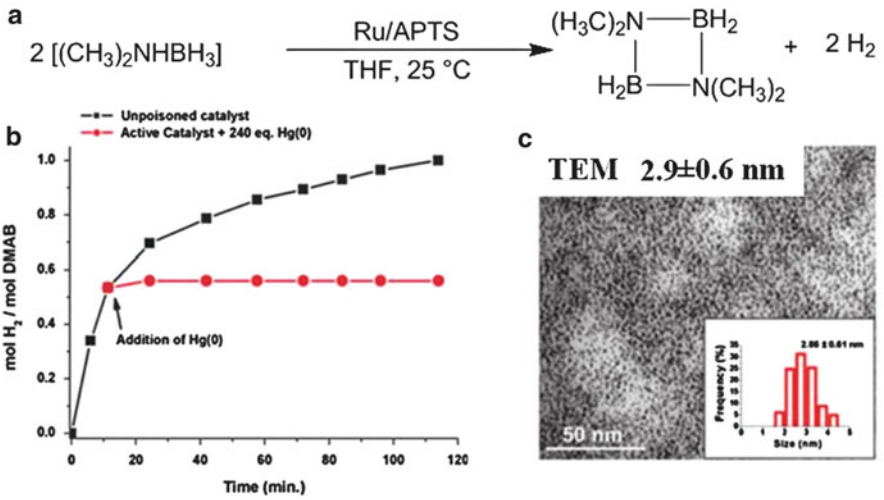

Fig. 16 (**a**) Dehydrogenation of dimethylamine-borane catalyzed by Ru/APTS NPs in THF at r.t. (**b**) mol H_2/mol DMAB vs. time graph ([Ru] = 2.24 mM; [DMAB] = 54 mM; 240 equiv. of Hg(0) after ~50% conversion of DMAB), and (**c**) TEM image of Ru/APTS NPs (~2.9 nm) after the third catalytic run. (Adapted from [104] with permission from RSC)

1.2–2.4 nm range. The catalytic performance of these Ru/APTS NPs was studied in the catalytic dehydrogenation of dimethylamine-borane (Me_2NHBH_3; DMAB) under mild conditions (Fig. 16a) [104, 105]. Following the addition of DMAB into a THF solution of Ru/APTS NPs, hydrogen evolution immediately started with an initial turnover frequency (TOF) of 53 h^{-1} and continued until 1 equiv. H_2 per mol DMAB was released. To determine the homogeneous or heterogeneous nature of the catalytic reactivity, Hg(0), a poison for heterogeneous metal(0) catalysts, was added into the reaction mixture. The suppression of the catalysis in the presence of Hg(0) demonstrated that the catalyst was heterogeneous: the reaction occurred at the surface of the nanoparticles (Fig. 16b). The initial TOF value of 53 h^{-1} obtained with this system was comparable to that of the prior best heterogeneous catalyst of rhodium nanoclusters (TOF = 60 h^{-1}). In addition, it was the first example of an isolable, bottleable, and reusable transition metal nanocatalyst for the dehydrogenation of dimethylamine-borane (Fig. 16c). An increase of APTS concentration resulted in a significant decrease of the catalytic activity as a result of a higher coverage of the metallic surface. The maximum catalytic activity was achieved with Ru/APTS = 3 which appeared as the best compromise between the NP mean size and the surface accessibility.

By varying the nature of the ligands used for the synthesis of RuNPs, we could obtain various colloidal solutions which are stable in organic media. Precise characterization by IR and NMR techniques allowed us to understand better how the ligand affects the characteristics of the obtained particles, such as their size, shape, and surface state. Depending on the strength of coordination of the ligands at

the metal surface, we can expect different nanostructures and consequently different surface properties. In summary, ligands which are strongly coordinated at the metal surface, such as phosphorus molecules and phenylpyridine, lead to very small and spherical RuNPs. On the contrary, amines and aminoalcohols are weakly coordinating ligands but this can be exploited to induce a specific morphology. Some of our RuNPs were investigated in colloidal catalysis leading to encouraging results although there is still a long way to go in the field of enantioselective catalysis. Since we can prepare various nanostructures displaying different surface chemistry, we now have different tools to deeply explore the world of well-defined nanocatalysts with the aim to find catalytic systems of high selectivity and activity in the near future.

4 Water-Soluble RuNPs for Investigation in Aqueous Colloidal Catalysis

Due to sustainability issues, we have been interested in the synthesis of water-soluble MNPs for their use as catalysts in water. For this purpose, we took inspiration from organometallic catalytic systems in water and considered ligands, such as 1,3,5-triaza-7-phosphaadamantane (PTA) and sulfonated diphosphines, which are frequently employed to stabilize complexes.

4.1 PTA-Stabilized RuNPs

PTA is a versatile ligand which combines a strong basicity and a very small cone angle to a high solubility in both organic solvents and water. The synthesis of PTA-stabilized RuNPs was carried out by decomposition of the [Ru(COD)(COT)] precursor in the presence of 0.8 equiv. of PTA ($P(H_2) = 3$ bar; THF; 70°C) (Fig. 17) [106, 107]. The resulting NPs displayed a spherical shape and low size dispersity, with a mean diameter of 1.3 nm. These NPs were purified by washing with pentane and filtration, and then dissolved in water with no change in dispersion and mean diameter (~1.4 nm). Aqueous suspensions of these NPs were stable for weeks under argon atmosphere. The coordination of the ligand at the Ru surface was investigated by NMR; ^{1}H, ^{13}C, ^{31}P solution and solid-state NMR studies showed the strong coordination of PTA at the surface of the particles via the phosphorous atom. DOSY experiments excluded the presence of exchange processes at the NMR time scale. In addition, PTA was not released following the addition of excess dodecanethiol, showing the strong interaction of PTA with the nanoparticles' surface. In the presence of air, an excess of PTA resulted in low quantity of PTA-oxide. Interestingly, in addition to the signals of PTA ligands, the ^{1}H MAS NMR spectrum of Ru@PTA showed a weak signal at −14 ppm which is a typical

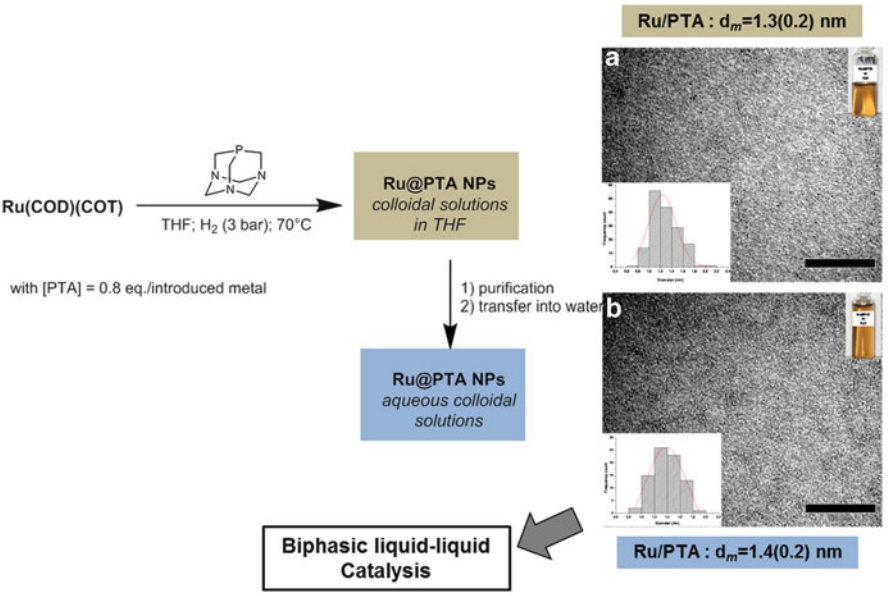

Fig. 17 Synthesis of PTA-stabilized RuNPs and TEM images in THF (*top*) and in water (*bottom*). (Adapted from [106] with permission from RSC)

value for hydrides. It is worth mentioning the disappearance of this peak following the exposure of the nanoparticles to air or deuterium atmospheres. As the presence of hydrides at the surface of various RuNPs was previously demonstrated through indirect methods as well as by static ^{2}D NMR, this peak was attributed to surface hydrides. For the first time hydrides were observed on the nanoparticles' surface via direct ^{1}H NMR.

In collaboration with Buntkowsky et al., ^{31}P–^{13}C REDOR NMR measurements allowed a reasonable approximation of distances between PTA ligands and carbon monoxide (CO) molecules on the surface of PTA-stabilized RuNPs following the adsorption of ^{13}CO on these particles [108]. REDOR data evidenced that ^{13}C and ^{31}P nuclei form complex spin systems with distributions of multiple dipolar couplings on the surface of the NPs. However, the ^{31}P and ^{13}C REDOR curves at short dephasing times are dominated by nearest neighbor interactions. This allowed us to determine the nearest neighbor distance between the PTA ligand and CO to be 3.1 Å, which is in good agreement with the results of quantum chemical DFT calculations about small cluster compounds. This work shed light on the interactions between CO and phosphine as well as on the binding geometries of these molecules on the surface of the RuNPs. As information on the ligand location and mobility is precious for the understanding of the chemical and catalytic properties of nanoparticles, these results support the interest of using sophisticated NMR tools to investigate the surface chemistry of nanoparticles.

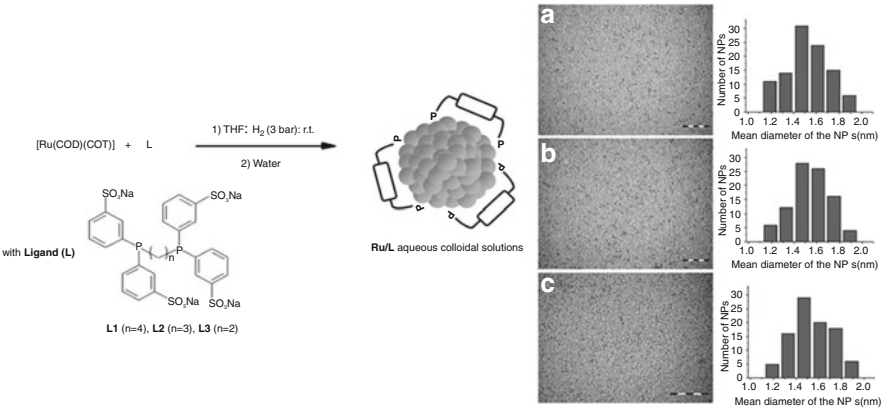

Fig. 18 Synthesis and TEM images of sulfonated diphosphine-stabilized RuNPs in water with (**a**) dppb-TS (**b**) dppp-TS, and (**c**) dppe-TS with [L]/[Ru] = 0.1. (Adapted from [109] with permission from Elsevier)

Finally, these aqueous colloidal solutions were used as catalysts for the hydrogenation of simple olefins and arenes with Roucoux et al. [107]. These nanocatalysts appeared efficient in mild conditions, evidencing that these materials are active despite the evolution of their environment related to their dissolution into water. For example, octene and dodecene were fully converted into the corresponding alkanes (r.t; 1 bar H_2) with moderate activities. An increase in the hydrogen pressure ($P(H_2) = 10$ bar) was not detrimental for the stability of the colloidal suspension. The complete hydrogenation of toluene into cyclohexane was observed overnight with Ru/PTA, whereas 60% of *m*-methoxymethylcyclohexane was formed from methoxymethylanisole. Nevertheless, preliminary recycling tests showed that an improvement of the stability and recovery of these materials was necessary to increase their interest in catalysis.

4.2 Sulfonated Diphosphine-Stabilized RuNPs

By applying the procedure previously described for PTA ligand, we used sulfonated diphosphines to stabilize RuNPs [109]. In this collaborative work with Roucoux and Monflier et al., the RuNPs were prepared from [Ru(COD)(COT)] and different diphosphines, (1,4-bis[(di-*m*-sulfonatophenyl)phosphine]butane = dppb-TS; 1,4-bis [(di-*m* sulfonatophenyl)phosphine]propane = dppp-TS; 1,4-bis[(di-*m* sulfonatophenyl) phosphine]ethane = dppe-TS) in THF (3 bar H_2; RT). Various ligand/Ru ratios were employed in order to analyze the effect of both the backbone and the diphosphine concentration on the stability, size, and catalytic properties of the NPs. Depending on the amount of ligand, this resulted in the formation of well-crystallized RuNPs which exhibit a mean size in the range of 1.2–1.5 nm (Fig. 18). The coordination of

Table 2 Hydrogenation of styrene with Ru/sulfonated diphosphine aqueous colloidal solutions and picture of the reaction medium. (Adapted from [109] with permission from Wiley)

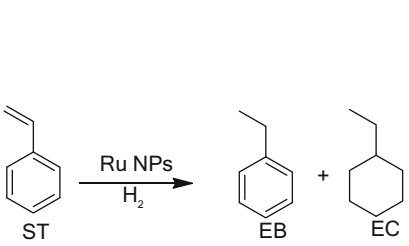

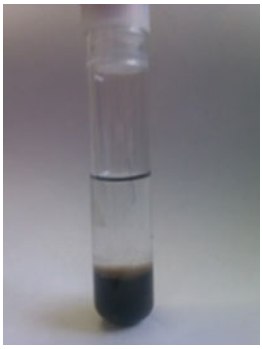

			Products selectivity (%)		
Nanocatalysts	*T* (°C)	Time (h)	ST	EB	EC
Ru/dppb-TS	20	1	25	75	0
	20	20	0	45	55
	20	40	0	3	97
Ru/dppp-TS	20	1	59	40	1
	20	20	0	47	53
	20	40	0	2	98
Ru/dppe-TS	20	1	75	24	1
	20	20	0	41	59
	20	40	0	1	99
Ru/dppb-TS	50	1	10	90	0
	50	2	0	82	18
	50	3	0	0	100

Reaction conditions: [Ligand]/[Ru] = 0.1; Ruthenium (3.9×10^{-5} mol), styrene (3.9×10^{-3} mol), 1 bar H_2, water (10 mL)

the sulfonated diphosphines at the surface of the RuNPs allowed their facile dispersion in water giving rise to very homogeneous and stable aqueous colloidal solutions (up to several months) with no change in their mean sizes.

The catalytic evaluation of these aqueous colloidal solutions showed promising reactivities for the hydrogenation of unsaturated substrates (tetradecene, styrene and acetophenone) in biphasic liquid–liquid conditions. Interestingly, minor structural differences in the diphosphine ligands, such as the alkyl chain length, influenced the catalytic activity in styrene hydrogenation in addition to the positive effect of temperature (from 20°C to 50°C) or pressure (from 1 to 10 bar H_2) increase (Table 2). As the [Ligand]/[Ru] ratio increased, conversion and selectivity (expressed as ethylbenzene (EB)/ethylcyclohexane (EC) ratio) also increased at short reaction times. The best results were obtained with the dppb-TS ligand which

exhibits the longest alkylchain giving rise to 75% EB after 1 h; dppp-TS led to 40% EB and dppe-TS resulted in the formation of 20% of EB. As all these RuNPs display similar mean sizes, their different performances in catalysis may result from different flexibilities of their alkyl chain. Due to the highest number of carbon atoms, dppb-TS ligand had the highest flexibility and therefore favored a better diffusion of the substrate towards the metal surface. Although the mean size (1.25 nm) of the RuNPs remained similar with the increase of [dppe-TS]/[Ru] from 0.2 to 0.5, an evolution of the selectivity is observed. The aromatic substrate could have a more limited access to the NP surface since the presence of a higher density of ligands coordinated to this surface increases the sterical hindrance. A molar ratio of 0.1 appeared to be a good compromise between the stabilization and catalytic activity of the NPs. Finally, as for Ru/PTA NP systems, preliminary studies offered encouraging results about the recovery of these water-soluble Ru/sulfonated disphosphine nanocatalysts. These results confirmed the high versatility of the organometallic approach for the synthesis of metal nanoparticles since efficient preparations of nanoparticles can be achieved to get in aqueous solutions.

4.3 Sulfonated Diphosphine/Cyclodextrin-Stabilized RuNPs

The combined presence of both a sulfonated diphosphine and a cyclodextrin (CD) led to very stable water-soluble RuNPs which displayed suitable performances in the catalytic hydrogenation of unsaturated substrates due to a supramolecular control effect of the cyclodextrin (Fig. 19) [110]. The so-obtained nanoparticles were fully characterized and compared to sulfonated diphosphine-stabilized RuNPs. Interestingly, deep NMR investigations evidenced: (1) the strong coordination of the sulfonated diphosphine ligand at the metallic surface, (2) in the presence of cyclodextrin, the formation of an inclusion complex between the sulfonated diphosphine and the cyclodextrin which modified the coordination mode of the diphosphine. Indeed, an interaction between the sulfonated diphosphine and the cyclodextrin was unambiguously observed by NMR spectroscopy (both in solution and in solid state). This interaction was even stronger at higher cyclodextrin content which hugely disrupted the coordination properties of the diphosphine on the metal surface. However, this interaction only took place when the cyclodextrin was present during the synthesis of the particles.

The catalytic properties of the sulfonated diphosphine-stabilized RuNPs and sulfonated diphosphine/cyclodextrin-stabilized RuNPs were compared in the hydrogenation of unsaturated model substrates (styrene, acetophenone, and *m*-methylanisole) in biphasic liquid–liquid conditions (i.e., ruthenium aqueous colloidal solution and organic substrate; no added solvent). Whilst all of these RuNPs displayed suitable performances in catalysis, different activities and selectivities were observed. This highlighted that supramolecular interactions on the metallic surface in the presence of a cyclodextrin control the catalytic reactivity of the nanocatalysts. Interestingly the CD acts as a phase-transfer promotor, which

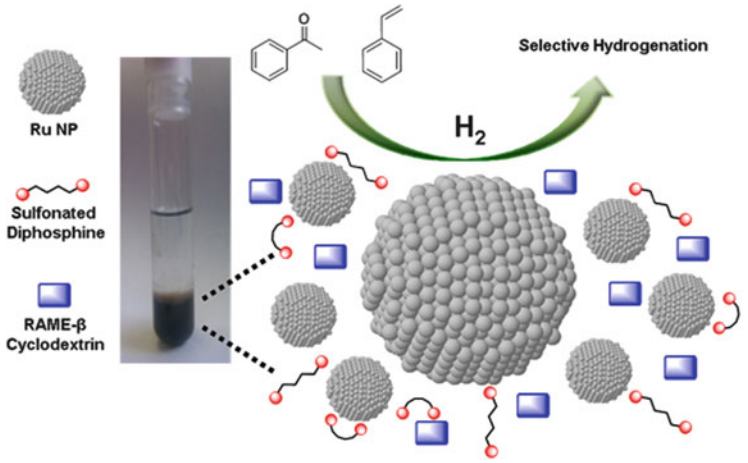

Fig. 19 RuNPs stabilized by a mixture of sulfonated diphosphine + Rame-β-cyclodextrin as selective catalyst for hydrogenation of styrene and acetophenone. (Reproduced from [110] with permission from Wiley)

increases the activity and affects the selectivity. As evidenced via NMR studies, the influence of CD on the selectivity may result from the formation of an inclusion complex between the CD and the diphosphine ligand at the RuNPs surface. This original work takes advantage of the supramolecular properties of a cyclodextrin to modulate the surface reactivity of diphosphine-stabilized RuNPs which is expected to offer novel opportunities to the field of nanocatalysis.

All these results point out the high versatility of the organometallic approach for the synthesis of metal colloidal solutions in aqueous media. The recent results obtained by combining organometallic complexes as precursors and hydrosoluble molecules as stabilizers open the way for catalytic applications in water. As previously reported using complexes in molecular chemistry, the catalytic performance of Ru nanocatalysts can be controlled at a supramolecular level in the presence of both a sulfonated diphosphine and a cyclodextrin. This highlights that metal nanoparticles can be considered as organometallic objects of large size; the surface chemistry of which can be modified by selecting the ligands similarly to molecular complexes.

5 Ionic Liquid-Stabilized RuNPs

Providing more environmentally friendly conditions than usual solvents, the use of ionic liquids (ILs), acting as both the solvent and the stabilizer, has emerged as an alternative for the preparation of nanocatalysts [22, 23, 111–113]. Both experiments and simulations reported in literature have evidenced the segregation phenomenon

that exists between polar and non-polar domains in imidazolium-based ILs [114, 115]. The organometallic synthesis of MNPs in ionic liquids has been initiated by Dupont et al. who followed our method to produce nanoparticles directly from organometallic precursors in the ILs [116–118]. This route is also applied by the group of Gomez [119, 120].

In collaboration with Santini et al., we investigated the stabilization of RuNPs in the presence of imidazolium-derived ionic liquids [121–126]. The synthesis of RuNPs was first performed in 1-butyl methylimidazoliumbis(trifluoromethanesulfonyl)imide ([RMIm][NTf_2]; R = C_4H_9) [121]. This implied to control the decomposition of [Ru(COD)(COT)] under 4 bar of H_2 without adding any further stabilizer. To study their influence on the NPs formed different temperatures of reaction (0°C and 25°C) and stirring rates were selected. At 25°C under stirring, homogeneously dispersed RuNPs were observed with a mean size of ~2.4 nm. At 0°C, the RuNPs, which had a smaller size of ~0.9 nm, tend to agglomerate to form larger clusters of 2–3 nm. When no stirring was applied at 0°C, the NPs displayed a slightly larger mean size, ~1.1 nm and no agglomeration was observed. These results showed the influence of the temperature on the mean size of the NPs: the smallest NPs were obtained at the lowest temperature. The size of RuNPs is governed by the degree of self-organization of the imidazolium-based ionic liquid. The 3D organization of the ionic liquid is better maintained at low temperature which led to a better confinement of the Ru nuclei and finally smaller nanoparticles.

This observation was further confirmed by using a series of imidazolium-derived ionic liquids: [RMIm][NTf_2] (R = C_nH_{2n+1} with $n = 2$; 4; 6; 8; 10), [R_2Im][NTf_2] (R = Bu) and [BMMIm][NTf_2] (with BMMIm = 1-butyl-2,3-dimethylimidazolium) [122]. In all of these ILs, the size of the RuNPs was smaller at 0°C than at 25°C, and the stirring induced their agglomeration. Additionally, the increase in alkyl chain lengths was found to be linearly proportional with the mean size of the RuNPs (Fig. 20). In parallel, simulation of the molecular dynamics evidenced a relationship between the size of IL non-polar domains and the mean diameter of RuNPs, which highlights the role of the organization of the ILs on the control of the RuNPs size. Crystal growth occurs inside the pockets created by the non-polar domains of the ILs, giving rise to a confinement effect which leads to the control of the growth of the particles. Finally, the addition of a polar solute like water to the ionic liquid induced the aggregation of the particles due to the disruption of the ionic liquid 3D structure.

The use of spectroscopic methods evidenced the presence of hydrides at the surface of the nanoparticles [123]. As part of the labeling experiments, H/D exchange was studied at the surface of the RuNPs prepared in 1-butyl-3-methylimidazolium bis(trifluorosulfonyl)imide by exposing the colloidal solution to a D_2 atmosphere. After several days, an analysis of the gas atmosphere by NMR revealed the formation of HD in agreement with the initial presence of hydrides on the ruthenium nanoparticles. The quantification of hydrides, by hydrogenation of ethylene at room temperature, gave a value of 0.6H/Ru_{surf}. In addition, the hydrides present at the surface of the particles display a stabilizing effect since a more important coalescence is observed under stirring in the presence of argon

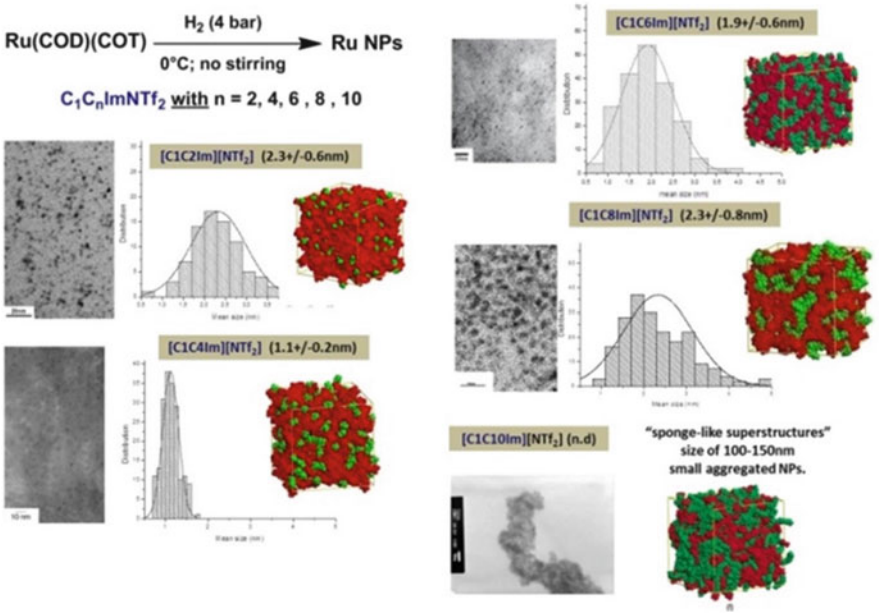

Fig. 20 Influence of the ionic liquid chain length on the size of the RuNPs. (Adapted from [122] with permission from RSC)

atmosphere instead of H_2 atmosphere. When the synthesis of the nanoparticles was performed under deuterium, an H/D exchange occurred for all of the carbons of the imidazolium ring. This shows that the RuNP surface is active and in the near environment of the side alkyl group (Fig. 21).

In addition, we studied the influence of the addition of amines on both the size control of IL-prepared RuNPs and the stability of these NPs [124, 125]. Whilst RuNPs are reference catalysts in hydrogenation reactions, IL-stabilized RuNPs are generally not stable in the conditions required for catalytic hydrogenation. For this study, the ionic liquids [RMIm][NTf_2] (R = C_nH_{2n+1}, $n = 2, 4, 6, 8, 10$) were used in the presence of octylamine (OA) or hexadecylamine (HDA) as additional ligands. The synthesis of the NPs was performed following the previously described conditions, and 0.2 M equiv. of the selected ligand. Regardless of the alkyl chain length of the IL, well-dispersed and well-crystallized NPs were obtained with a mean size in the range of 1.1–1.3 nm (Fig. 22). These RuNPs displayed a better size dispersity than the corresponding RuNPs only stabilized with an amine ligand [61]. Whilst IL prevents particles from agglomeration through a confinement effect, amines also play an important role in controlling the size and dispersion of these NPs. This demonstrates the interest of using ionic liquids to confine nanoparticles in the non-polar domains (*nanoreactors*) in the presence of a ligand which stabilizes the particles at a very small size.

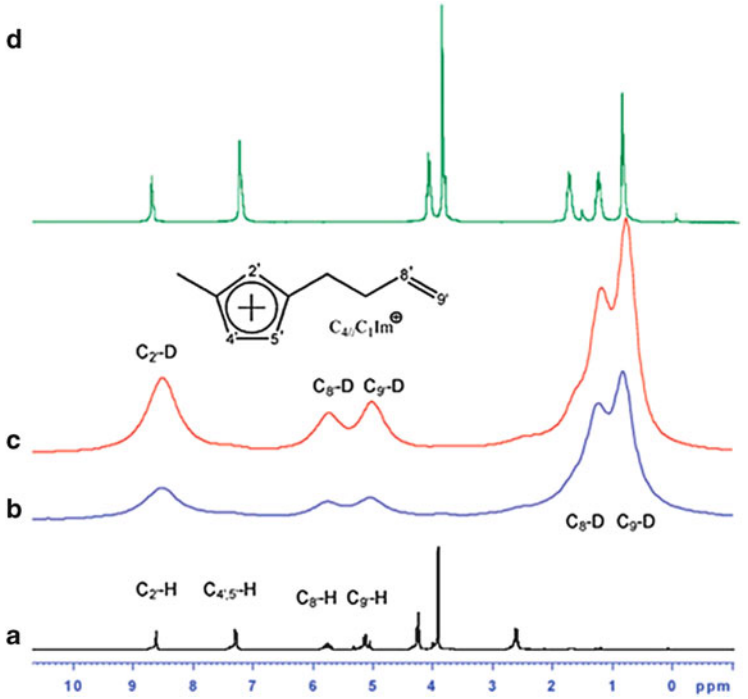

Fig. 21 (**a**) ^{1}H NMR spectra of C_4//C_1Im NTf_2, neat IL_2; (**b**) ^{2}H NMR spectra of IL_2 after RuNP formation at 0°C under deuterium; (**c**)^{2}HNMR spectra of IL_2 after RuNP formation at 50°C under deuterium; (**d**) ^{1}H NMR spectra of C_4C_1Im NTf_2, neat. (Reproduced from [123] with permission from RSC)

Hydrogenation of toluene was first performed at different temperatures with the RuNPs synthesized in $C_1C_4ImNTf_2$ in the presence of octylamine, (Table 3). The conversion obtained was low but reproducible. A temperature of 75°C was then selected to evaluate the catalytic properties of the Ru colloids. Since Ru/HDA and Ru/OA have similar size and shape, the slightly lower conversion obtained by hexadecylamine was explained by viscosity changes in the reaction mixtures and by a higher steric hindrance of HDA once coordinated on the RuNP surface.

These systems were also tested in the hydrogenation of 1,3-cyclohexadiene (CYD), styrene (STY), and R-(+)-limonene (LIM). Whilst the activity of the RuNPs in these hydrogenation reactions increased with σ-donor ligands, such as $C_8H_{17}NH_2$ and H_2O, a decrease of the activity was observed using bulkier and π-acceptor ligands, i.e. $PPhH_2$ PPh2H and CO. This underlined the quasi-molecular nature of sub-3 nm NPs since their activity can be tuned by the σ-π-ligand character similarly to homogeneous catalysis.

In summary, imidazolium-based ILs display a high degree of self-organization in the liquid state. Both theoretical and experimental studies showed that a three-dimensional ionic network dominated by electrostatic interactions coexists with

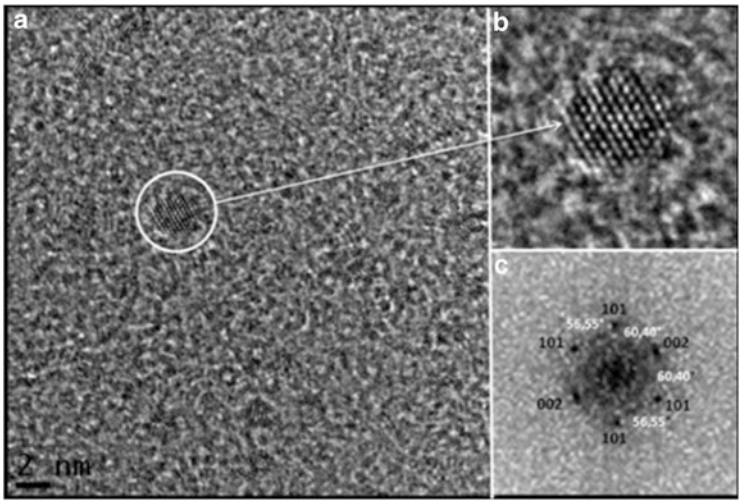

Fig. 22 (**a**) General HREM image of *C4OA*-stabilized RuNPs in $C_1C_4ImNTf_2$, (**b**) HREM image of an isolated and well-crystallized *C4OA*-stabilized RuNP with (**c**) FFT. (Reproduced from [124] with permission from RSC)

Table 3 Hydrogenation of toluene with RuNPs synthesized in $C_1C_4ImNTf_2$ + octylamine. (Reproduced from [124] with permission from RSC)

Nanocatalyst IL/ligand	T (°C)	PhMe/ Ru_T	PhMe/ Ru_S	Ru_S/ Ru_T	Conversion (%)	TON[a]	$k_{initial}$[b]
C4OA	30	38/1	46/1	0.82	4	2	
C4OA	50	38/1	46/1	0.82	9	4.5	
C4OA	75	38/1	46/1	0.82	17	8	12 ± 1
C4OA	100	38/1	46/1	0.82	17	8	
C4HDA	75	38/1	52/1	0.73	14	6.5	
C4OA	75	38/1	46/1	0.82	17	8	12 ± 1
C6OA	75	38/1	49/1	0.77	16	8	8 ± 1
C8OA	75	38/1	49/1	0.77	11	5.5	5 ± 1
C10OA	75	38/1	52/1	0.73	14	7	7 ± 1

Reaction conditions: $P(H_2) = 1.2$ bars; reaction time = 5 h; Ru_T = total amount of Ru atoms; Ru_S = amount of surface Ru atoms
[a]Turn over number (moles of product converted per mol of Ru_S)
[b]Estimated initial rates in 10^{-2} mol L^{-1} h^{-1}

non-polar domains resulting from the lipophilic alkyl side chains. Due to a confinement effect, this phenomenon facilitated the growth control of the RuNPs. The catalytic performance of these RuNPs was further improved via the addition of an amine as co-stabilizer. As expected, the amine played an important role in controlling the size, shape, and stability of the RuNPs.

6 Investigation of RuNPs in Supported Catalysis

In the last 15 years, the application of supported metal nanoparticles as catalysts in organic synthesis has received a renewed interest. The association between a metal and a support could result in synergistic effects which would precisely drive the reactivity of these nanocatalysts, e.g. supported-gold NPs for the oxidation of carbon monoxide [127]. The recyclability and recovery from the reaction medium still remains one of the major drawbacks to a widespread use of NPs in catalysis. To overcome these problems, the immobilization of MNPs on solid supports appears as a promising alternative. Synthetic methods are also developed to achieve the direct synthesis of MNPs in the presence of a support in a controlled manner. Intensive work is made on the functionalization of the support to increase the anchorage of the particles, inspired by the ligands which are used to stabilize MNPs in solution.

The organometallic approach for the synthesis of MNPs can also be applied for the preparation of composite materials. Some results were obtained using alumina membranes, mesoporous silica, and carbon materials as templates for the deposition of MNPs, mainly for hydrogenation and oxidation reactions. Metal oxide ruthenium nanoparticles could be obtained after a calcination step on the preformed nanoparticles under air without change in size and dispersion. The inclusion of MNPs was performed following two different approaches: (1) either by impregnation of the support using a colloidal solution of preformed NPs or (2) by direct synthesis of the nanoparticles in the presence of the support, with or without a ligand.

6.1 Alumina-Supported RuNPs for Hydrogenation and Oxidation Reactions

In a collaborative work with Schmid et al., the filling of nanoporous alumina membranes of various pore widths was carried out in two different ways from the decomposition of [Ru(COD)(COT)] in THF/MeOH mixtures in the absence of stabilizer [128]. The first approach involved the impregnation of alumina support with colloidal solutions of RuNPs of different sizes which were dependent on the ratio of MeOH/THF in the reaction mixture. Colloidal solutions were transferred into membranes by vacuum induction. Only a few agglomerates were observed outside of the pores whereas dense areas were located within the membrane channels. The second approach consisted of the room-temperature decomposition of [Ru(COD)(COT)] under 3 bar of H_2 following the deposition of this metal precursor inside the pores. In this way, homogeneous materials displaying well-dispersed RuNPs were obtained in the pores of alumina membranes. The size of the particles depended on the pore diameter of the template. These materials were evaluated in two catalytic reactions, i.e. the hydrogenation of 1,3-butadiene and

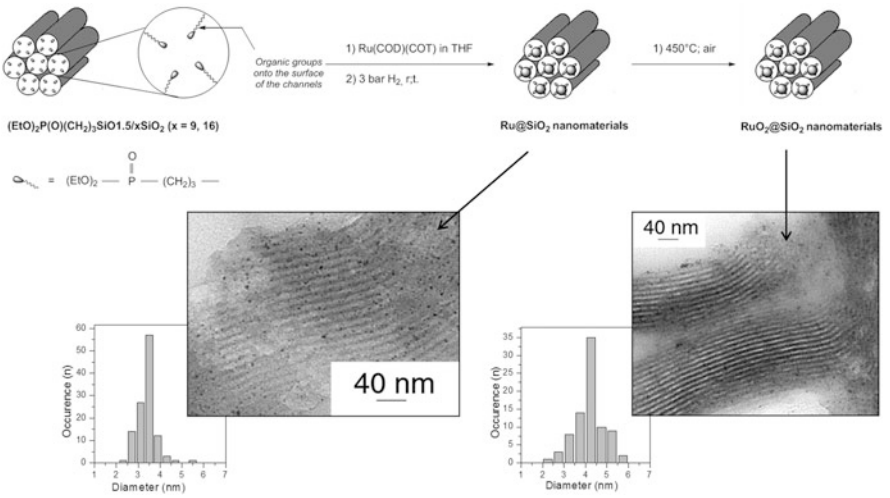

Fig. 23 Synthesis and TEM images of Ru and RuO_2NPs inside the pores of a phosphonate-functionalized mesoporous silica. (Adapted from [130] with permission from Wiley)

the gas-phase oxidation of CO [129]. For both reactions the decrease of the particle size resulted in an increase of activity.

6.2 *Silica-Supported RuNPs for Oxidation of Carbon Monoxide and Benzylalcohol*

In collaboration with Corriu et al., organized mesoporous silica materials containing phosphonate groups were used as a host for controlling the growth of RuNPs [130]. [Ru(COD)(COT)] was first impregnated into the support and then decomposed (3 bar H_2; RT). The phosphonate groups present in the pores of the solid acted as a stabilizer for the Ru/SiO_2 NPs which allowed their organization in the channels of the host material. A calcination step (air; 400°C) led to RuO_2/SiO_2 nanomaterial (Fig. 23). The use of RuO_2/SiO_2 composite nanomaterials, as catalytic filters for gas sensors, has been successful since these materials efficiently achieved the preferential detection of propane in a propane/CO/NO_2/air mixture. The sensitivity of the propane sensing was dependent on the metal content of the nanocomposite materials: higher Ru/Si_w induced higher S_{C3H8}/S_{CO} sensitivity ratios. The RuO_2/SiO_2 nanomaterials partially removed CO from the gas mixture via the selective oxidation of CO into CO_2, while the hydrocarbon content remained unaltered.

To control the size of the NPs inside the silica matrix, the organometallic approach was combined with the sol–gel method for the preparation of RuO_2/SiO_2 nanocomposite materials (Fig. 24) [131]. The key-point of this new

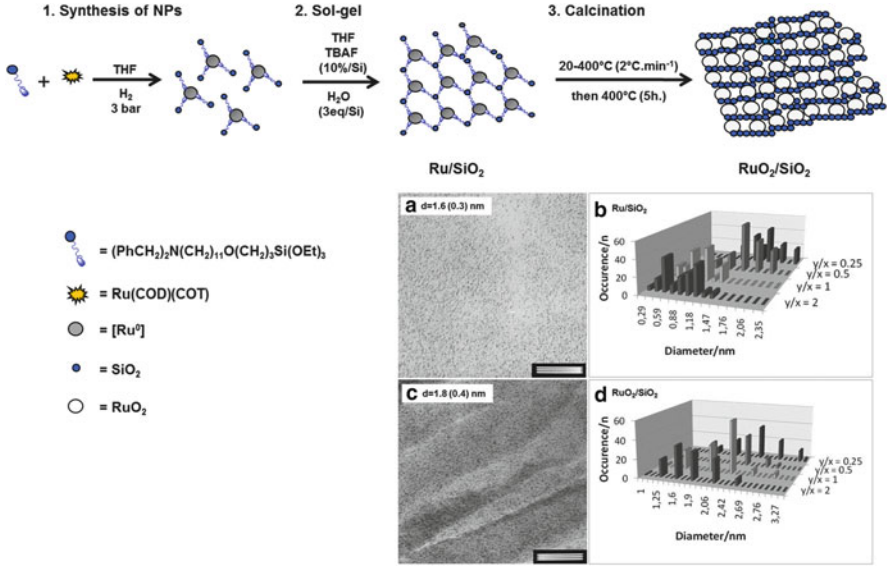

Fig. 24 Synthesis of Ru and RuO_2 NPs embedded in silica using a polycondensable amine; (**a**) TEM image of Ru/SiO_2 nanocomposites with L/Ru(COD)(COT) ratio of 2. (**b**) Distribution histograms of Ru/SiO_2 NPs. (**c**) TEM image of RuO_2/SiO_2 NPs with L/Ru(COD)(COT) ratio of 0.5. (**d**) Distribution histograms of RuO_2/SiO_2 nanocomposites with L/Ru(COD)(COT) = 2, 1, 0.5, 0.25 (Scale bars of TEM images = 50 nm). (Adapted from [131] with permission from Wiley)

methodology was to use a ligand ($(PhCH_2)_2N(CH_2)_{11}O(CH_2)_3Si(OEt)_3$; benzenemethanamine; L) which plays a double role: (1) a stabilizing agent for the synthesis of NPs, (2) a precursor for the silica matrix. This approach led to hybrid materials with high Ru contents, displaying well-dispersed and small size RuNPs in the silica matrix. A calcination step (air; 400°C) gave rise to mesoporous silica materials containing RuO_2 NPs. The mean size of the NPs was related to the [L]/[Ru(COD)(COT)] ratio. In addition, the addition of tetraethylorthosilicate (TEOS) to the initial [L]/[Ru(COD)(COT)] solution led to materials which exhibit higher proportions of silica and higher specific surface areas. These hybrid nanomaterials displayed a good dispersion inside the silica matrix and interesting surface-specific area properties, which made them attractive materials to be used as catalytic filters for gas sensors. This has been illustrated by an interesting increase of the sensitivity for the detection of propane.

Once adapted to 3-aminopropyltriethoxy-silane and 11-aminoundecyl-triethoxysilane, this methodology gave rise to very small and reactive RuO_2 NPs [132]. Studies in the aerobic oxidation of benzyl alcohol showed promising results for further development of this type of nanomaterials.

6.3 Carbon Material-Supported RuNPs for Hydrogenation and Oxidation Reactions

Carbon materials are often used for the immobilization of MNPs as these solid supports offer multiple advantages including easy availability, relatively low cost, high mechanical strength and chemical stability. In addition, their porous structure makes them attractive for surface chemistry since important modifications can be simply achieved, e.g. the facile functionalization of these materials favors the immobilization of the NPs.

In a collaborative work with Serp et al., we studied how the confinement of MNPs inside carbon nanotubes (CNTs) may influence their catalytic properties. Using CNTs with various functionalization, the synthesis of RuPtL/CNTs (L = 4-(3-phenylpropyl)pyridine) was performed, in different conditions of reaction, from a couple of organometallic precursors, i.e. [Ru(COD)(COT)] and [$Pt(CH_3)_2$(COD)](Fig. 25) [133]. One option consisted in the preparation of the NPs through the stabilization by the ligand first and then their impregnation on the CNTs. An alternative route was the co-decomposition of the two organometallic precursors in the presence of both the ligand L and the CNTs. The best results in terms of confinement of the particles were obtained by the impregnation method employing amide-functionalized CNTs. The resulting hybrid material had ~2–2.5 nm NPs which were located inside the CNTs (80% of NPs for a 23 wt.% of metal). In addition to the non-supported RuPt/L NPs, all of the prepared systems were evaluated as catalysts in the hydrogenation of cinnamaldehyde (Table 4). The catalytic activity and the selectivity of CNTs-supported RuPt/L NPs were higher than those of the non-supported NPs. For the NPs mainly located inside the CNTs, a remarkable selectivity towards the formation of cinnamyl alcohol was achieved.

In another work, NP/carbon hybrid systems were obtained by the impregnation of different mesoporous carbons with colloidal solutions of RuNPs previously prepared by the decomposition of [Ru(COD)(COT)], ($P(H_2) = 3$ bar; THF) in the presence of 4(3-phenylpropyl)pyridine ligands [134]. The supported RuNPs were well dispersed on the carbon materials with a mean size of 1.2–1.3 nm. These hybrid systems were successfully used as catalysts in the oxidation of benzyl alcohol in water at 80°C, giving rise to excellent conversion and selectivity (>99%) towards the aldehyde. The catalytic activity of these systems was found to be influenced by the hydrophilicity of the carbon support.

7 Conclusions and Perspectives

During the past decade, the design and characterization of ligand-stabilized metal nanostructures have experienced a huge development for their application in catalysis. The association between a metal core and a stabilizing ligand to form nanohybrids can be considered as crucial to control the surface properties of these

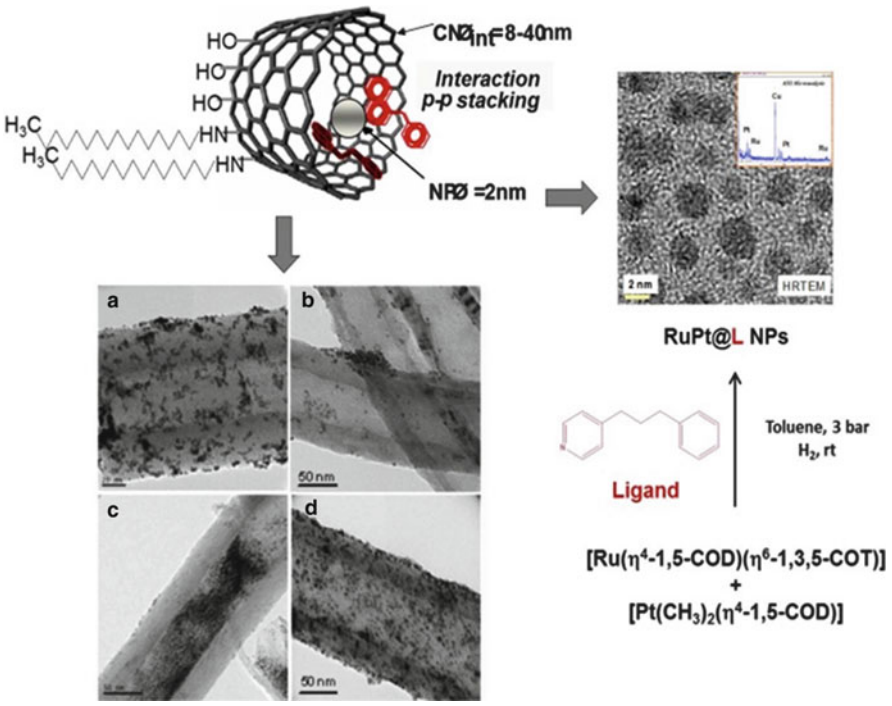

Fig. 25 *Top left*: Schematic representation of the confinement of the RuPt NPs in the channels of the CNTs. *Bottom left*: TEM images of the RuPt/L/CNTs nanomaterials with (**a**) 11% w/w PtRu/L/CNT, (**b**) 5% w/w PtRu/L/CNT-COOH, (**c**) 23% w/w PtRu/L/CNT-CO-NH-R (impregnation), and (**d**) 5% w/w PtRu/L/CNT-COOH (direct decomposition). *Right*: Synthesis and HREM image of the RuPt/L NPs. (Adapted from [133] with permission from Wiley)

nanostructures and their catalytic performance. Whilst a wide range of ligands can be used as stabilizers, their selection is guided by the similarity between the behavior of ligands on molecular complexes and on nanoparticles. This chapter overviews our contributions in this field giving representative results on ruthenium nanoparticles of interest in catalysis both in solution and in supported conditions, mainly for hydrogenation reactions. These results highlight our recent achievements in the field of ruthenium nanostructure to: (1) control their characteristics such as size, composition, surface state, solubility in organic or aqueous media, and deposition onto supports, (2) characterize their surface chemistry, and (3) explore their chemical properties using these nanoparticles as nanocatalysts.

In summary, we have over the years investigated a wide range of ligands on the surface of ruthenium nanoparticles. The first conclusion is that the behavior of ligands is similar on these nanoparticles and on molecular complexes. Thus, hydrides and CO coordinate on the surface of these nanoparticles, as well as olefins and methyl groups. The hydrides are always fluxional whereas CO appears only fluxional when the surface of the particles is free. Amines are also fluxional and do

Table 4 Catalytic hydrogenation of cinnamaldehyde with RuPt/CNTs nanomaterials. (Adapted from [133] with permission from Wiley)

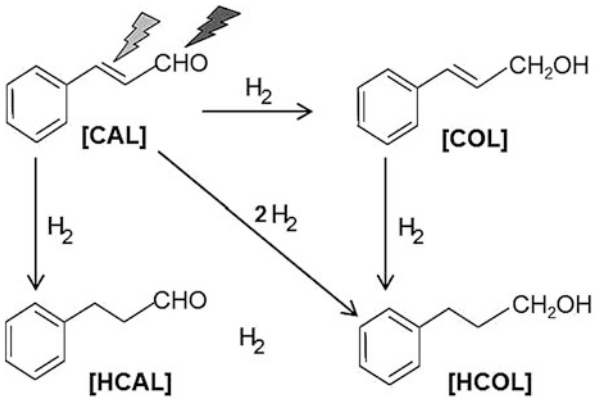

Catalyst	NPs d_{mean} (nm) $^{inside/outside}$	% NP int.	TOF (h^{-1})	HCAL	HCOL	COL
PtRu/L NPs	2,2	–	30	50	15	35
PtRu/CNT2	2,2/2,2	10	56	33	8	59
PtRu/CNT1	1,6/2,2	30	75	18	12	69
PtRu/CNT3	2/2,5	80	85	0	5	95

Reaction conditions: isopropanol; 20 bar H_2; 343 K; 2 h

not stabilize the particles unless they are added in excess. However, what is a drawback in molecular chemistry can be used here as an advantage since amines allow the growth of nanoparticles. This may lead to shape-controlled nano-objects, as reported by other groups. Phosphines and N-heterocyclic carbenes are, as in molecular chemistry, very promising since their steric and electronic properties can be modulated. Consequently, phosphines and N-heterocyclic carbenes are suitable ligands to precisely control the surface chemistry of the nanostructures, and further tune their properties. Using the same principle, hydrosoluble molecules can favor the dissolution of organometallic nanoparticles into aqueous media with no change in size, dispersion, or surface reactivity. This paves the way towards application in sustainable nanocatalysis. In addition, bimetallic, such as nano-objects alloys, core-shell or heterostructures, can also be prepared. Finally, the organometallic approach provides nanostructures which exhibit a "clean" surface since the only molecules coordinated to the surface are selected for the synthesis of these nanoparticles. As a consequence, these systems are suitable for precisely studying the properties of the ligands coordinated to the particle surface and the influence of the ligands on the properties of the nanoparticles' surface. For this purpose, in combination to other techniques, the nuclear magnetic resonance spectroscopy is a very helpful tool, well known in molecular chemistry to characterize precisely molecules and complexes. About the immobilization of nanoparticles on supports, the most promising results evidenced the important role of the functionalization of the support to increase the

anchorage of the particles. This improves the catalytic performances of these nanoparticles, such as selectivity, and facilitates the recovery of the catalyst.

On the basis of our long experience, i.e. 25 years, here exemplified with different metals, mainly ruthenium, we can affirm that the concepts and techniques of organometallic chemistry allow the design of nano-objects which display remarkable surface properties. This chapter describes new organometallic objects covered by different species: hydrides, CO, ancillary ligands, such as phosphines or N-heterocyclic carbenes. The location and dynamics of the ligands can be studied as well as the influence of the ligand location on the surface reactivity of the NPs. Due to advances in the field of characterization, including NMR techniques, the full characterization of the surface of catalytically active nanoparticles could be achieved at the molecular level. This achievement would drive the emergence of a complex chemistry on the surface of nanoparticles.

Recent results illustrate the possibility to perform selective chemistry on the surface of nanoparticles. Whilst we started with simple ligands (i.e., the hydride-carbonyl-phosphine triad which was the basis of the molecular organometallic chemistry in the 1970s), it is now required to develop both an understanding of this chemistry in collaboration with theoretical chemists and a more complex chemistry leading to highly selective transformations. Considering the recent advances, and predicting even more progress in the understanding of the formation and surface properties of NPs, we propose that future developments will provide novel hybrid nanocatalysts of interest in catalysis. Whilst other well-known methods often use commercially available metal sources, the organometallic approach requires the synthesis of the metal precursors. Even if an additional step may be perceived as a drawback, this efficient method is very complementary to other possibilities. The organometallic method is a highly versatile approach which is particularly attractive for its ability to afford precise control over the characteristics of nanostructures (size dispersion, chemical composition) and surface properties.

In terms of perspectives, many challenges remain to be met in nanocatalysis. The first one is probably the understanding of the influence of ligands on the course of catalytic reactions, e.g. how ligands could modify the selectivity of selected reactions. This would help in the preparation of nanocatalysts displaying catalytic performance of desire. Although numerous efforts have already been done with various capping agents all over the world, future progress will probably require the design of molecules more appropriate for the metal surface. As a consequence, it will be possible to produce nanoparticles designed for specific applications in catalysis. In this respect, one of the most interesting and challenging fields is asymmetric catalysis. Only a few examples of enantioselective reactions are presently known to be catalyzed by nanoparticles. Another area of importance is the activation and functionalization of C–H bonds which has been studied in heterogeneous catalysis and is rapidly developing in homogeneous catalysis. However, although nanoparticles seem to be perfectly fitted for these reactions, this field remains to be explored. However, recent results in the regioselective and stereospecific isotopic labeling of nitrogen-containing compounds may open a new way

for organic chemistry. Finally, for sustainable development issues, the recycling and the recovery of the nanocatalysts are also to be improved.

Acknowledgments All our collaborators are greatly acknowledged for their fruitful contributions. We also thank CNRS, University Paul Sabatier at Toulouse University, Institut des Sciences Appliquées at Toulouse (INSA), the Midi-Pyrénées region (including CTP program), ANR (SIDERUS-ANR-08-BLAN-0010-03; SUPRANANO-ANR-09-BLAN-0194), ANR-DFG (MOCA-NANO-ANR-11-INTB-1011 and DFG-911/19-1), INTERREG SUDOE (TRAIN 2 project), EU (ARTIZYMES STREP-FP6-2003-NEST-B3-0151471; SYNFLOW FP7-NMP2-Large program 2010–246461; NANOSONWINGS ERC Advanced Grant-2009-246763), CAPES-COFECUB, CONACyt, ANRT and Sasol for financial supports.

References

1. Schmid G (ed) (1994) Clusters and colloids. From theory to applications. Wiley, Weinheim
2. Schmid G (ed) (2004) Nanoparticles. From theory to application. Wiley, Weinheim
3. Zhou B, Han S, Raja R, Somorjai G (eds) (2003) Nanotechnology in catalysis. Kluwer Academic/Plenum Publisher, New York
4. Ulrich H, Uzi L (eds) (2007) Nanocatalysis. Series Nanoscience and Technology. Springer Berlin and Heidelberg
5. Roucoux A, Philippot K (2007) In: de Vries JG, Elsevier CJ (eds) Handbook of homogeneous hydrogenations, vol 9. Wiley, Weinheim, pp 217–255
6. Astruc D (ed) (2008) Nanoparticles and catalysis. Wiley-Interscience, New York
7. Somorjai GA, Frei H, Park JY (2009) J Am Chem Soc 131:16589–16605
8. Somorjai GA, Aliaga C (2010) Langmuir 26:16190–16203
9. Somorjai GA, Park JY (2009) Surf Sci 603:1293–1300
10. Somorjai GA, Li Y (2010) Top Catal 53:311–325
11. Zhang Y, Grass ME, Kuhn JN, Tao F, Habas SE, Huang W, Yang P, Somorjai GA (2008) J Am Chem Soc 130:5868–5869
12. Cushing BL, Kolescnichenko VL, O'Connor CJ (2004) Chem Rev 104:3893–3946
13. Tao AR, Habas S, Yang P (2008) Small 4:310–325
14. Pradhan SM, Pal T (2010) J Colloid Interface Sci 341(2):333
15. Mourdikoudis S, Liz-Marzán LM (2013) Chem Mater 25:1465
16. Guyonnet Bilé E, Cortelazzo-Polisini E, Denicourt-Nowicki A, Sassine R, Launay F, Roucoux A (2012) ChemSusChem 5:91
17. Grubbs RB (2007) Polym Rev 47(2):2015
18. Yan N, Zhang J, Yuan Y, Chen G-T, Dyson PJ, Li Z, Kou Y (2010) Chem Commun 46:1631
19. Myers VS, Weir MG, Carino EV, Yancey DF, Pande S, Crooks RM (2011) Chem Sci 2:1632
20. Astruc D (2003) CR Chimie 6:709
21. Astruc D, Diallo AK, Ornelas C (2013) In: Serp P, Philippot K (eds) Nanomaterials and catalysis. Wiley, Weinheim, Chap 3, p 101
22. Dupont J, Scholten JD (2010) Chem Soc Rev 39:1780
23. Scholten JD, Prechtl MG, Dupont J (2012) Handbook of green chemistry, vol 8. Wiley, Weinheim, p 1
24. Nag A, Kovalenko MV, Lee J-S, Liu W, Spokoyny B, Talapin DV (2011) J Am Chem Soc 133:10612–10620
25. Philippot K, Chaudret B (2003) CR Chim 6:1019–1034
26. Baumer M, Libuda J, Neyman KM, Rosch N, Rupprechterz G, Freund H-J (2007) Phys Chem Chem Phys 9:3541–3558
27. Corma A, García H (2008) Chem Soc Rev 37:2096–2126

28. Risse T, Shaikhutdinov S, Nilius N, Sterrer M, Freund H-J (2008) Acc Chem Res 41:949–956
29. Freund H-J (2010) Chem Eur J 16:9384–9397
30. Nilius N, Risse T, Schauermann S, Shaikhutdinov S, Sterrer M, Freund H-J (2011) Top Catal 54:4–12
31. Primo A, Corma A, García H (2011) Phys Chem Chem Phys 13:886–910
32. Serna P, Boronat M, Corma A (2011) Top Catal 54:439–446
33. Boronat M, Corma A (2011) J Catal 284:138–147
34. López C, Corma A (2012) ChemCatChem 4:751–752
35. Chaudret B, Commenges G, Poilblanc R (1982) J Chem Soc Chem Commun 1388–1390
36. Cormary B, Dumestre F, Liakakos N, Soulantica K, Chaudret B (2013) Dalton Trans 42:12546–12553
37. Amiens C, Chaudret B, Ciuculescu-Pradines D, Colliére V, Fajerwerg K, Fau P, Kahn M, Maisonnat A, Soulantica K, Philippot K (2013) New J Chem 37:3374–3401
38. Gregson D, Howard JAK, Murray M, Spencer JL (1981) J Chem Soc Chem Commun 716
39. Frost PW, Howard JAK, Spencer JL, Turner DG (1981) J Chem Soc Chem Commun 1104
40. Chaudret B, Cole-Hamilton DJ, Wilkinson G (1978) J Chem Soc Dalton Trans 1739
41. Philippot K, Chaudret B (2003) C R Acad Sci 6:1019
42. Vranka RG, Dahl LF, Chini P, Chatt J (1969) J Am Chem Soc 91:1574–1576
43. Fumagalli A, Martinengo S, Chini P, Albinati A, Bruckner S, Heaton BT (1978) J Chem Soc Chem Comm 195–196
44. Washecheck DM, Wucherer EJ, Dahl Lawrence F, Ceriotti A, Longoni G, Manassero Mario M, Sansoni M, Chini P (1979) J Am Chem Soc 101:6110–6112
45. Scott SL, Susannah, Basset JM (1994) J Mol Catal 86:5–22
46. Schmid G, Boese R, Pfeil R, Bandermann F, Meyer S, Calis GHM, van der Velden JWA (1981) Chem Ber 114:3634
47. Wallenberg LR, Bovin JO, Schmid G (1985) Surf Sci 156:256–264
48. Van Staveren MPJ, Brom HB, De Jongh LJ, Schmid G (1986) Solid State Comm 60:319–322
49. Benfield RE, Creighton JA, Eadon DG, Schmid G (1989) Zeitschrift fuer Physik D Atoms Mol Clusters 12:533–536
50. Schmid G (1990) Inorg Synth 7:214–218
51. Bradley JS, Hill EH, Leonowicz ME, Wirzke H (1987) J Mol Catal 41:59–74
52. Philippot K, Chaudret B (2007) Comprehensive organometallic chemistry III. In: Crabtree RH, Mingos MP (Eds-in-Chief) Volume 12 – Applications III: functional materials, environmental and biological applications, Dermot O'Hare (Volume Ed.), Chapter 12–03, Elsevier, Oxford, pp 71–99
53. Mehdaoui B, Carrey J, Stadler M, Cornejo A, Nayral C, Delpech F, Chaudret B, Respaud M (2012) App Phys Lett 100:052403/1
54. Barriere C, Piettre K, Latour V, Margeat O, Turrin C-O, Chaudret B, Fau P (2012) J Mater Chem 22:2279
55. Meffre A, Lachaize S, Gatel C, Respaud M, Chaudret B (2011) J Mater Chem 21:13464
56. Dumestre F, Chaudret B, Amiens C, Fromen M-C, Casanove M-J, Renaud P, Zurcher P (2002) Angew Chem Int Ed 41(22):4286
57. Wetz F, Soulantica K, Respaud M, Falqui A, Chaudret B (2007) Mater Sci Eng C 27:1162
58. Schmid G (2010) In: In: Schmid G (ed) Nanoparticles from theory to applications. Second completely revised and updated edition. Wiley, Weinheim, p 217
59. Bradley JS, Millar JM, Hill EW, Behal S, Chaudret B, Duteil A (1991) Faraday Discuss 92:255–268
60. Duteil A, Quéau R, Chaudret B, Mazel R, Roucau C, Bradley JS (1993) Chem Mater 5:341–347
61. Pan C, Pelzer K, Philippot K, Chaudret B, Dassenoy F, Lecante P, Casanove M-J (2001) J Am Chem Soc 123:7584–7593
62. Novio F, Philippot K, Chaudret B (2010) Catal Lett 140:1–7

63. Pieters G, Taglang C, Bonnefille E, Gutmann T, Puente C, Berthet J-C, Dugave C, Chaudret B, Rousseau B (2014) Angew Chem Int Ed 53:230–234
64. Vidoni O, Philippot K, Amiens C, Chaudret B, Balmes O, Malm J-O, Bovin J-O, Senocq F, Casanove M-J (1999) Angew Chem Int Ed 38:3736–3738
65. Pelzer K, Vidoni O, Philippot K, Chaudret B, Collière V (2003) Adv Funct Mater 13:118–126
66. Pelzer K, Philippot K, Chaudret B (2003) Z Phys Chem 217:1–9
67. Lara P, Philippot K, Chaudret B (2013) ChemCatChem 5:28–45
68. Sun S, Fullerton EE, Weller D, Murray CB (2001) IEEE Trans Magn 37:1239–1243
69. Metin O, Mazumder V, Ozkar S, Sun S (2010) J Am Chem Soc 132:1468–1469
70. Liu Y, Wang C, Wei Y, Zhu L, Li D, Jiang JS, Markovic NM, Stamenkovic VR, Sun S (2011) Nano Lett 11:1614–1617
71. Watt J, Yu C, Chang SLY, Cheong S, Tilley RD (2013) J Am Chem Soc 135:606–609
72. Lignier P, Bellabarba R, Tooze RP, Su Z, Landon P, Ménard H, Zhou W (2012) Cryst Growth Des 12:939–942
73. Ramirez E, Jansat S, Philippot K, Lecante P, Gomez M, Masdeu-Bulto AM, Chaudret B (2004) J Organomet Chem 689:4601–4610
74. García-Antón J, Axet MR, Jansat S, Philippot K, Chaudret B, Pery T, Buntkowsky G, Limbach HH (2008) Angew Chem Int Ed 47:2074–2078
75. Novio F, Monahan D, Coppel Y, Antorrena G, Lecante P, Philippot K, Chaudret B (2014) Chem Eur J 20:1287–1297
76. Favier I, Massou S, Teuma E, Philippot K, Chaudret B, Gomez M (2008) Chem Commun 3296–3298
77. Jansat S, Gomez M, Philippot K, Muller G, Guiu E, Claver C, Castillon S, Chaudret B (2004) J Am Chem Soc 126:1592–1593
78. Favier I, Gomez M, Muller G, Axet MR, Castillon S, Claver C, Jansat S, Chaudret B, Philippot K (2007) Adv Synth Catal 349:2459–2469
79. Weitz DA, Huang JS, Lin MY, Sung J (1985) Phys Rev Lett 54:1416
80. Favier I, Lavedan P, Massou S, Teuma E, Philippot K, Chaudret B, Gómez M (2013) Top Catal 56:1253–1261
81. Vignolle J, Tilley TD (2009) Chem Commun 7230–7232
82. Lara P, Rivada-Wheelaghan O, Conejero S, Poteau R, Philippot K, Chaudret B (2011) Angew Chem Int Ed 50:12080–12084
83. Gonzalez-Galvez D, Lara P, Rivada-Wheelaghan O, Conejero S, Chaudret B, Philippot K, van Leeuwen PWNM (2013) Catal Sci Technol 3:99–105
84. Wang D, Li Y (2011) Adv Mater 23:1044
85. Zeng H, Sun S (2008) Adv Funct Mater 18:391
86. Jun Y-W, Choi J-S, Cheon J (2007) Chem Commun 12:1203
87. Cozzoli PD, Pellegrino T, Manna L (2006) Chem Soc Rev 35:1195
88. Bradley JS, Hill EW, Chaudret B, Duteil A (1995) Langmuir 11:693
89. Pan C, Dassenoy F, Casanove M-J, Philippot K, Amiens C, Lecante P, Mosset A, Chaudret B (1999) J Phys Chem B 103:10098
90. Dassenoy F, Casanove M-J, Lecante P, Pan C, Philippot K, Amiens C, Chaudret B (2001) Phys Rev B 63:235407
91. Lara P, Casanove M-J, Lecante P, Fazzini P-F, Philippot K, Chaudret B (2012) J Mater Chem 22:3578
92. Lara P, Ayvali T, Casanove M-J, Lecante P, Fazzini P-F, Philippot K, Chaudret B (2013) Dalton Trans 42:372
93. Kelsen V, Meffre A, Fazzini P-F, Lecante P, Chaudret B (2014) ChemCatChem. doi:10.1002/cctc.201300907
94. Bonnefille E, Novio F, Gutmann T, Poteau R, Lecante P, Jumas J-C, Philippot K, Chaudret B (2014) Nanoscale. doi:10.1039/C4NR00791C
95. Baddeley CJ, Jones TE, Trant AG, Wilson K (2011) Top Catal 54:1348–1356

96. Jansat S, Picurelli D, Pelzer L, Philippot K, Gomez M, Muller G, Lecante P, Chaudret B (2006) New J Chem 30:115–122
97. Gual A, Axet MR, Philippot K, Chaudret B, Denicourt-Nowicki A, Roucoux A, Castillón S, Claver C (2008) Chem Commun 2759–2761
98. Gonzalez-Galvez D, Nolis P, Philippot K, Chaudret B, van Leeuwen PWNM (2012) ACS Catal 2:317–321
99. Ackermann L (2006) Synthesis 1557–1571
100. Ackermann L, Born R, Spatz JH, Althammer A, Gschrei CJ (2006) Pure Appl Chem 78:209–214
101. Wolpers A, Ackermann L, Vana P (2010) Macromol Chem Phys 212:259–265
102. Rafter E, Gutmann T, Löw F, Buntkowsky G, Philippot K, Chaudret B, van Leeuwen PWNM (2013) Catal Sci Technol 3:595–599
103. Stephens FH, Pons V, Baker RT (2007) Dalton Trans 25:2613–2626
104. Zahmakıran M, Philippot K, Özkar S, Chaudret B (2012) Dalton Trans 41:590–598
105. Zahmakiran M, Tristany M, Philippot K, Fajerwerg K, Özkar S, Chaudret B (2010) Chem Commun 46:2938–29540
106. Debouttière PJ, Martinez V, Philippot K, Chaudret B (2009) Dalton Trans 10172–10174
107. Debouttière PJ, Coppel Y, Denicourt-Nowicki A, Roucoux A, Chaudret B, Philippot K (2012) Eur J Inorg Chem 1229–1236
108. Gutmann T, Bonnefille E, Breitzke H, Debouttière P-J, Philippot K, Poteau R, Buntkowsky G, Chaudret B (2013) PCCP 15:17383–17394
109. Guerrero M, Roucoux A, Denicourt-Nowicki A, Bricout H, Monflier E, Collière V, Fajerwerg K, Philippot K (2012) Catal Today 183:34–41
110. Guerrero M, Coppel Y, Chau NTT, Roucoux A, Denicourt-Nowicki A, Monflier E, Bricout H, Lecante P, Philippot K (2013) ChemCatChem 12:3802–3811
111. Yan N, Xiao C, Kou Y (2010) Coord Chem Rev 254:1179–1218
112. Hallett JP, Welton T (2011) Chem Rev 111:3508–3576
113. Pârvulescu VI, Hardacre C (2007) Chem Rev 107:2615–2665
114. Pádua AAH, Costa Gomes MC, Canongia Lopes JNA (2007) Acc Chem Res 40:1087–1096
115. Pensado AS, Pádua AAH (2011) Angew Chem Int Ed 50:8683–8687
116. Prechtl MHG, Scariot M, Scholten JD, Machado G, Teixeira SR, Dupont J (2008) Inorg Chem 47:8995–9001
117. Prechtl MHG, Scholten JD, Dupont J (2009) J Mol Chem 313:74–78
118. Scholten JD, Leal BC, Dupont J (2012) ACS Catal 2:184–200
119. Raluy E, Favier I, Lopez-Vinasco AM, Pradel C, Martin E, Madec D, Teuma E, Gomez M (2011) Phys Chem Chem Phys 13:13579–13584
120. Rodriguez-Perez L, Pradel C, Serp P, Gomez M, Teuma E (2011) ChemCatChem 3:749–754
121. Gutel T, Garcia-Anton J, Pelzer K, Philippot K, Santini CC, Chauvin Y, Chaudret B, Basset JM (2007) J Mater Chem 17:3290–3292
122. Gutel T, Santini CC, Philippot K, Padua A, Pelzer K, Chaudret B, Chauvin Y, Basset J-M (2009) J Mat Chem 19:3624–3631
123. Campbell PS, Santini CC, Bouchu D, Fenet B, Philippot K, Chaudret B, Padua AAH, Chauvin Y (2010) Phys Chem Chem Phys 12:4217–4223
124. Salas G, Santini CC, Philippot K, Colliere V, Chaudret B, Fenet B, Fazzini PF (2011) Dalton Trans 40:4660–4668
125. Salas G, Podgorsek A, Campbell PS, Santini CC, Padua AAH, Gomes MFC, Philippot K, Chaudret B, Turmine M (2011) Phys Chem Chem Phys 13:13527–13536
126. Salas G, Campbell PS, Santini CC, Philippot K, Costa Gomes MF, Padua AAH (2012) Dalton Trans 41:13919–13926
127. Bond GC, Louis C, Thompson DT (2006) Catalysis by gold. Imperial College Press, London
128. Pelzer K, Philippot K, Chaudret B, Meyer-Zaika W, Schmid GZ (2003) Anorg Allg Chem 629:1217–1222

129. Kormann H-P, Schmid G, Pelzer K, Philippot K, Chaudret B (2004) Z Anorg Allg Chem 630:1913–1918
130. Jansat S, Pelzer K, García-Antón J, Raucoules R, Philippot K, Maisonnat A, Chaudret B, Guari Y, Medhi A, Reyé C, Corriu RJP (2007) Adv Funct Mater 17:3339–3347
131. Matsura V, Guari Y, Reyé C, Corriu RJP, Tristany M, Jansat S, Philippot K, Maisonnat A, Chaudret B (2009) Adv Funct Mater 19:3781–3787
132. Tristany M, Philippot K, Guari Y, Collière V, Lecante P, Chaudret B (2010) J Mater Chem 20:9523–9530
133. Castillejos E, Debouttière P-J, Roiban L, Solhy A, Martinez V, Kihn Y, Ersen O, Philippot K, Chaudret B, Serp P (2009) Angew Chem Int Ed 48:2529–2533
134. García-Suárez EJ, Tristany M, García AB, Collière V, Philippot K (2012) Micropor Mesopor Mater 153:155–162